

34 dissolved LNAPL to the receiving receptors. The mass transfer coefficient value of $9.50E-02$;
35 $5.80E-03$; $3.50E-03$; $1.20E-04$ m/s was estimated for rapid, general, slow and stable
36 groundwater table conditions, respectively. Furthermore, the estimated Sherwood numbers (Sh)
37 were found 0.95, 16.20, 16.95 and 19.30 while Peclet numbers (Pe) were 1.80, 75.47,
38 80.14, and 95.06 for rapid, general, slow and stable cases respectively. This shows that the
39 dissolution is highly affected by groundwater table which may cause loss of pollutant mass as
40 a dissolved phase. However, the transport of dissolved LNAPL plume is comparatively fast in
41 case of rapid fluctuating groundwater, resulting in closely spaced concentration isolines of
42 toluene containing plume. A high biodegradation rate is observed in plume regions having
43 concentration ranges from 140-160 ppm, while it decreases in the plume regions having high
44 concentrations (>160 ppm) and low concentrations (<140 ppm) in these cases. In sand tank,
45 the microbial growth was found to be increasing as plume moves away from the LNAPL pool
46 towards low-gradient, which fortifies detrimental impact of toluene on survival of indigenous
47 microorganisms near the LNAPL pool. The results of this study may help in implementing
48 effective remediation technique to decontaminate LNAPL polluted sites under fluctuating
49 groundwater table conditions, especially in (semi)-arid coastal aquifers.

50

51 **Keywords:** LNAPL, Groundwater fluctuation, Dissolution, Biodegradation, 2D tank
52 experiments, Numerical modeling

53

54 **1. Introduction**

55 The subsurface contamination by LNAPL is widespread and challenging environmental
56 problem, especially in coastal regions having dynamic groundwater table condition due to tidal
57 effects. Most of the petroleum industries and refineries are located in coastal regions. The
58 leakage of LNAPL from subsurface storage tanks and disposal sites of effluents (Nema and
59 Gupta, 1999; Kumar et al. 2016) on surface are major source of hydrocarbons pollution of the
60 receiving environment, especially under varying subsurface conditions. When LNAPL is
61 released into (sub)-surface, it starts moving downward through the partially saturated zone, in
62 response to gravitational force, until it reaches to the capillary fringe (Das and Mirzaei, 2012;
63 Power et al. 1992a, b; 1994a, b; Illangasekare et al. 1995). A fraction of LNAPL mass is being
64 retained in partially saturated zone and LNAPL-air mass partition (i.e. volatilization process)
65 contributes as vapor phase contamination (Nambi and Powers, 2000; Brusseau et al. 2002,
66 Nambi and Powers, 2003, Patterson and Davis, 2009). The remaining pool of LNAPL provides

67 sufficient dissolving area to the underlying groundwater in smear zone which starts dissolving
68 with flowing groundwater and create a dissolved phase plume (Lee and Chrysikopoulos, 1998;
69 Kim and Chrysikopoulos, 1999; Nema and Gupta, 2003; Oostrom et al. 2006; 2007). Molecular
70 diffusion and mechanical dispersion along with advective flux cause spreading of dissolved
71 plume to downgradient receiving locations (Das, 2002; Yadav and Hassanizadeh, 2011; Picone
72 et al. 2013). On the other hand, native potential microbes play significant role to degrade the
73 dissolved LNAPL from polluted zone (Yadav et al. 2013; Basu et al. 2015, Mustapha et al.
74 2018).

75 Groundwater flow regimes play a significant role in the dissolution of pure phase
76 LNAPL pool and its movement to the surrounding locations (Das and Nassehi, 2003; Dobson
77 et al. 2007; Sulaymon and Gzar, 2011, Kamaruddin et al. 2011; Yadav et al. 2012). Dynamic
78 nature of groundwater table causes significant spreading of pooled LNAPL in smear zone,
79 which considerably increases the LNAPL-water interphase area and resulted in accelerated
80 dissolution (Mobile et al. 2012; Vasudevan et al. 2014). Variations in groundwater table not
81 only causes changes in the soil-water system, but also impacts the LNAPL pool behavior, if it
82 is present on the water table and in the underlying saturated zone. The LNAPL lying on the top
83 of the groundwater table moves down with it when the water table lowers and leave a trail of
84 LNAPL in the unsaturated zone in the form of isolated ganglia. Subsequently when the
85 groundwater table rises, the LNAPL pool also moves upward leaving behind a trapped amount
86 of LNAPL in the form of disconnected blobs in the saturated zone (Lenhard et al. 2004;
87 Kechavarzi et al. 2005). A part of the residual LNAPL in unsaturated zone gets mobilized again
88 when the groundwater table rises. Thus, a dynamic groundwater table accelerates the
89 dissolution of pure phase LNAPL resulting in high concentration of LNAPL plume (Legout et
90 al. 2009). The dissolved LNAPL plume then moves along with groundwater and forms a
91 polluted zone which features with varying concentration levels (Neale et al. 2000; Rolle et al.
92 2009; Zhang et al. 2014; Zhou et al. 2015; Sarikurt et al. 2017).

93 There is a paucity of knowledge on the impact of dynamic groundwater table conditions
94 on LNAPL behaviors in subsurface. Groundwater fluctuation is significantly affected by heavy
95 pumping rates to irrigate agricultural land and concurrent recharge due to return flow. Typically
96 for shallow aquifers, a high pumping rates and return flow/recharge may cause rapid fluctuation
97 of groundwater table. While, a slow pumping and less return flow/recharge may lead to
98 general/slow groundwater table fluctuation. Different nature of rainfall events is also
99 responsible for such a rapid and slow fluctuation of groundwater table. Fluctuations in the
100 groundwater table due to various reasons including tidal effects have a profound influence on

101 the spatial distribution, dissolution and biodegradation of LNAPL in the subsurface
102 environment. This phenomenon is predominantly observed in shallow aquifer regions where
103 most of the petrochemical industries and refineries are located and potentially at high risk of
104 LNAPL release from the subsurface storage tanks. Thus, an extensive study was conducted to
105 investigate LNAPL fate and transport under fluctuating groundwater table conditions using a
106 series of 2-D sand tank experiments. A better understanding of fate and transport of LNAPL
107 under varying subsurface water table condition is required which in turn can help in designing
108 effectively remediation technologies and to accurately predict their clean-up times and the
109 associated cost.

110

111 **2. Materials and Methods**

112 In this study, the behavior of pooled pure phase LNAPL and its dissolved plume in subsurface
113 under stable and fluctuating groundwater table conditions is investigated using a series of two-
114 dimensional laboratory experiments and numerical modelling. The preliminary experiments
115 were conducted to characterize the flow and transport parameters of the developed
116 subsurface soil-water system. Mechanical sieve analysis was performed to find the
117 particle size distribution of the sand which is listed in Table 1 along with other physical
118 parameters. The porosity of sand packing was determined using oven dry and volumetric
119 methods. Further, the hydraulic conductivity of the system was estimated using a constant
120 head permeameter. To see the behavior of the pooled LNAPL and dissolved phase plume, a
121 series of two dimensional sand tank experiments were performed by considering varying
122 groundwater table conditions. A two dimensional sand tank setup filled with homogenous sand
123 was used to conduct the laboratory experiment under (1) steady-state groundwater condition
124 and (2) three different dynamic groundwater table fluctuation conditions, separately. Lastly,
125 the soil-water system was numerically simulated using HYDRUS 2D model considering the
126 laboratory investigated soil-water and solute transport parameters.

127

128

129

130

131

132

133

134

Table 1. Properties of the sand used in the laboratory experiments.

Characteristic	Values
Type	Medium Sand
Grain Size	0.5-1 mm
Particle Size > 1 mm	1.71±0.5%
Particle Size 0.5mm-1mm	98.27±0.5%
Particle Size < 0.5 mm	0.02±0.01%
Effective Porosity	0.33±0.02%
Bulk Density	1.52 ±0.1g/cm ³
Grain Density	2.31±0.1 g/cm ³

136

137 **2.1 Two Dimensional Sand Tank Setup**

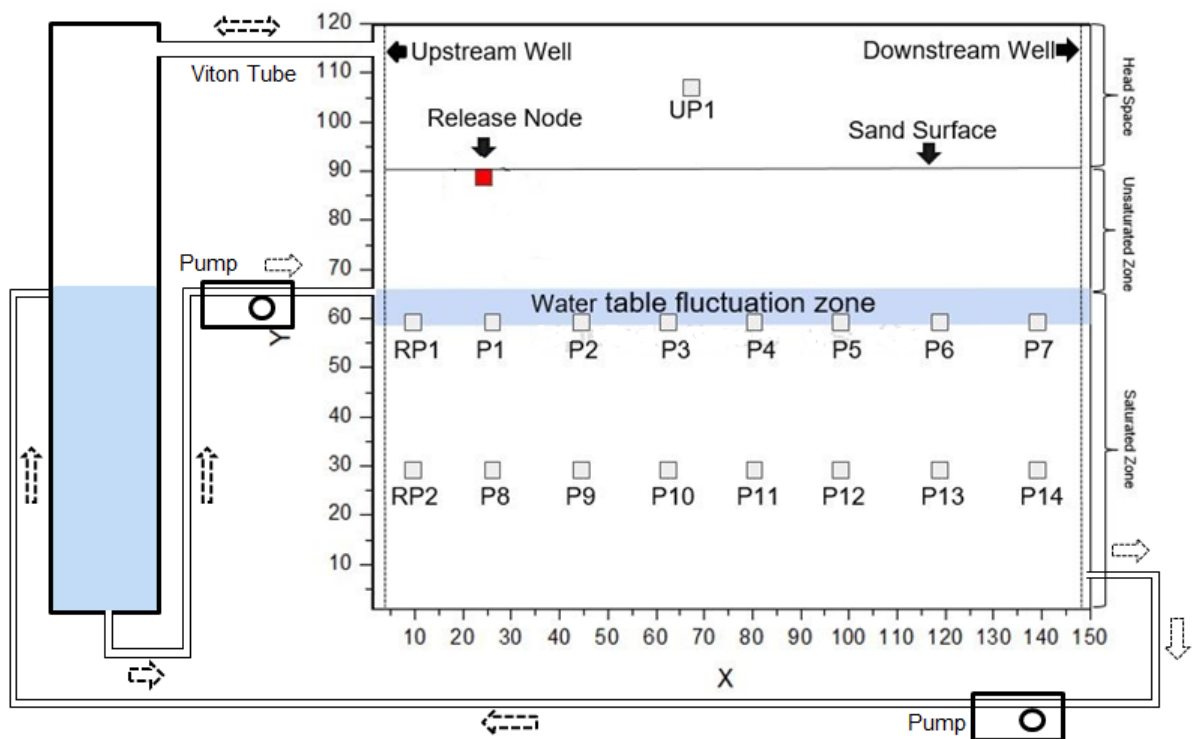
138 Two dimensional sand tank setup used in the study was specially designed using 2.5 mm thick
 139 stainless steel formed box with inner dimensions of 150 cm-long × 120 cm-high ×10 cm-deep
 140 (Figure 1). Two wells were installed at each side of tank and front cover of the tank was made-
 141 up of a thick glass sheet for enabling observations. Indian standard clean sand (650 grade-II)
 142 of particle size 0.5-1mm free from organic matter was packed in the central chamber between
 143 both the wells up to a height of 90 cm. The top 30 cm thick sand pack was kept as head-space
 144 to maintain aerobic condition. The porous media was oversaturated before pouring it into the
 145 column setup to create a homogenous packing. During this filling, a comb-like metallic tool
 146 was used to smooth the sand surface for avoiding a layered structure of the porous media. The
 147 extra water was then gravitationally drained out from the bottom of tank setup. The system was
 148 then flushed at maximum velocity until the effluent water was free of suspended fine material.
 149 After each of the experiments, the used sand was replaced with fresh sand pack the new set of
 150 the experiments following the packing procedure as describes earlier. The wells were used as
 151 upstream (high pressure) and downstream (low pressure) reservoir to maintain the water table.
 152 An auxiliary column containing the collected groundwater was connected to the inlet port of
 153 upstream well with viton tubes of a peristaltic pump. This peristaltic pump refers as “upstream
 154 pump” was used to supply the groundwater to the sand tank through the upstream well. The
 155 objective of this auxiliary column was to provide sufficient groundwater storage required to
 156 maintain the dynamic groundwater table conditions (Figure 1a). Similarly, the outlet of the

157 downstream well was connected to another peristaltic pump (refer herein as downstream pump)
158 to extract the groundwater and recirculate to the auxiliary column. The flow rate of the pumps
159 was adjustable so that the desired pressure difference in the two reservoirs can be maintained
160 and thereby controlling the groundwater flow within the tank setup. A LNAPL release port was
161 installed just below the top surface of sand packing about 20 cm from the upstream well. The
162 sampling ports having equal horizontal spacing of 15.5 cm are situated at 30 and 60 cm height
163 from the bottom of the tank setup in two horizontal layers (figure 1b). Piezometers were
164 attached to the tank to measure the positions of the groundwater table during experiments.
165 Filtration screens were fixed around the inlet and outlet valves to prevent the entrance of the
166 sand particles in the connecting viton tubes.

167 A series of tracer transport experiments were performed to determine the longitudinal
168 and vertical dispersivity of sand under fast, base and slow groundwater velocities. A solution
169 of tap water and sodium chloride with an initial concentration of 1000 mg/l was continuously
170 injected to the tank for the selected groundwater fluctuation cases. The water samples were
171 routinely collected from the sampling port located at 50 cm away (at X:45; Y:50 cm) in the
172 lower-gradient side from the injection port of the top sampling layer and the tracer
173 concentrations were measured using portable conductivity meter. The longitudinal dispersivity
174 (D_L) resulted from the dispersivity flux were estimated using the breakthrough curves (BTCs)
175 obtained from the tracer experiments. Time values corresponding to relative concentration
176 ratios of 84%, 50%, and 16% were used in calculating the dispersion coefficient (D_L) and
177 longitudinal dispersivity (α_L) as proposed by Sulaymon and Gzar (2011). In the equation,
178 $D_{ij} = \tau D_* + D_x$, the first term resulted from diffusive flux was estimated by multiplying the
179 diffusion coefficient of toluene i.e. 6.3×10^{-6} [cm²/sec] and tortuosity of sand i.e. 1.43
180 (Sulaymon and Gzar, 2011). The vertical dispersivity (D_v) were considered 0.1 times of the
181 obtained longitudinal dispersivity (Dobson et al. 2007).

182 A series of LNAPL transport experiments were performed using 2D sand tank setup for
183 stable/steady and three different groundwater table level conditions. Under steady-state
184 condition, a constant groundwater flux was applied as inflow (using the upstream pump) and
185 the same was extracted as outflow (using the down-stream pump) to maintain a constant flow
186 velocity in the horizontal direction and, hence, keeping the water table location at a constant
187 height. However, in rapid, general and slow groundwater level fluctuation experiments the
188 inflow/outflow flux were controlled by peristaltic pump to maintain a raising of the water

189 table by 5cm in 1, 2, and 4 hours respectively. The groundwater table was then lowered
 190 in the same manner; a drop of 5 cm was achieved in subsequent 1, 2 and 4 hours for rapid,
 191 general and slow fluctuation conditions, respectively. It may be noted herein that “one
 192 fluctuation cycle” refers to a complete high-low-high cycle of groundwater table levels.
 193
 194



195
 196 Figure 1. Schematic diagram of 2D sand tank setup integrated with an auxiliary column
 197 used to investigate fate and transport of LNAPL in subsurface under dynamic
 198 groundwater table conditions.
 199

200 Rising of groundwater table was maintained by pumping the water from the
 201 auxiliary column to the upstream well and closing the outflow from the downstream well
 202 for a target duration of respective fluctuation conditions. Likewise, groundwater falling
 203 was maintained by extracting water from the downstream well and closing the inflow to
 204 the sand tank from the auxiliary column for the same duration. Such switching of the
 205 peristaltic pump was adjustable and calibrated for a target duration of respective
 206 fluctuation conditions. A brief pumping details of different considered cases are listed in
 207 Table 2. To maintain a rise and fall of 5 cm, (150 cm-long \times 05 cm-magnitude of fluctuation
 208 \times 10 cm-deep \times 33% porosity) 0.002475 m³ or 2.475 liters of groundwater was required as
 209 inflow and outflow. Pure phase toluene was released from the top surface of the tank set up

210 to create a pool of the LNAPL above the groundwater table which was varied in the range of
 211 55-60 cm level from the tank bottom. The toluene (Merck with 99.9 % purity) was injected
 212 at a constant rate of 02 ml/min for a duration of 5 minutes using an air-tight syringe.
 213 Periodically, a small amount of soil water samples from both the layers and the soil vapor
 214 samples from head-space were collected carefully for the analysis.

215

216 Table 2. Inflow and outflow pumping strategies of groundwater table fluctuation cases.

Conditions	Inflow		Outflow		Total Duration	Pumping Rate
	Pumping		pumping			
	Rise	Fall	Rise	Fall		
Rapid fluctuation	1 hour	×	×	1 hour	2 hours	2475.0 mL/hr
General fluctuation	2 hours	×	×	2 hours	4 hours	1237.5 mL/hr
Slow fluctuation	4 hours	×	×	4 hours	8 hours	618.7 mL/hr

217
218

219 2.2 Sample Analysis

220 Soil water samples were collected periodically using needles attached with syringes
 221 (Hamilton gold) from the sampling ports embedded in the sampling layers in saturated zone
 222 (Figure 1). The samples were transferred into vials (Agilent vials: Agilent Product No.
 223 5190/1599) having air tight red septa caps without any air contacts. Similarly, soil vapor
 224 samples were collected from sampling ports installed in the headspace. The collected
 225 samples were analyzed using Gas chromatography-mass spectrometry (GC-MS) (Agilent
 226 7890B) in triplicates. A chrompack capillary column (30m×0.25mm, Silicone coating of
 227 0.25µm) was used for toluene analysis. Helium was employed as the carrier gas at a flow rate
 228 of 25 mL/min. Similarly, air and nitrogen were used with a flow rate of 20 mL/min during GC-
 229 MS analysis. During the measurements, temperature of injection port, oven, and detector port
 230 was kept at 150°C, 120°C, and 150°C, respectively. One set of collected samples were also
 231 analyzed using gas chromatography/combustion/isotope ratio mass spectrometry
 232 (GC/C/IRMS) technique to capture pure phase LNAPL (Dempster et al. 1997).

233

234

235 2.3 Microbiological Analysis

236 The microbial population in the soil water zone was counted using heterotrophic or
237 standard plate count methods (No. 9215C). In this method, colony forming units (CFU)
238 for live heterotrophic bacteria was estimated from the collected soil-water samples during
239 laboratory experiments. The soil water samples for microbial population count were
240 collected from M1 and M7 ports of top layer and M8 and M14 ports of bottom layer (Fig
241 2). After the sample collection, all the collected samples were diluted with a factor of 10^1
242 to 10^{-5} and mechanically shaken for 15 seconds. Growth media was prepared using a
243 combination of 20g protease peptone; 1.5g of K_2HPO_4 ; 1.5 g of $MgSO_4 \cdot 7H_2O$; and 20g of
244 Agar. Final pH of media was adjusted to 7.2 by adding 1N NaOH, before autoclaving at $121^{\circ}C$
245 for 15 minutes. The laminar air flow setup was wiped with the 70% ethanol and UV light for
246 the 15 minutes to avoid any background microbial contaminations. Well marked (sample
247 number, dilution, and date) plates were poured with 30mL prepared growth media and kept
248 still for few minutes to solidify agar surface. Thereafter, diluted samples were inoculated with
249 the help of spreader on agar surface of respective plates. Successively, all the plates were
250 incubated for 48 hours at $36 \pm 1^{\circ}C$ for. After the incubation, colony was counted manually using
251 the quadrature method. Plates having an un-countable number (or too numerous) was considered
252 as overgrowth. In this study, microbial populations were counted with the 12 hours'
253 interval to see the impact of LNAPL transport on microbial growth under fluctuating
254 groundwater table conditions. Thus, above mentioned microbial counting procedures
255 were performed for each experiments separately. A comparative account of such bacterial
256 count during groundwater table fluctuation experiments gives a clear idea on how
257 groundwater fluctuating conditions affects the LNAPL fate and transport in the
258 subsurface.

259

260 3. Numerical Modeling

261 To solve the dissolved phase LNAPL transport in saturated zone 2D form of mass balance
262 equation used as:

$$263 \quad \frac{\partial}{\partial t}(nS_f C_{if}) = -\nabla \cdot (q_f C_{if}) + \nabla \cdot (nS_f D_{if} \cdot \nabla C_{if}) + K_{if} - S \quad (1)$$

264 Where C_{if} is NAPL compound in f phase [ML^{-3}], q_f is discharge through soil profile [LT^{-1}],
265 n is porosity of soil [L^3L^{-3}], t is time [T], K_{if} is the dissolution rate of LNAPL [$ML^{-3}T^{-1}$] was
266 observed using characteristic length of LNAPL pool and equilibrium concentration in dissolved

267 phase. Likewise, S is biodegradation rate [$\text{ML}^{-3}\text{T}^{-1}$] (as sink term) was obtained using (control
268 and live) microcosms experiments. D_{if} is hydrodynamic dispersion [L^2T^{-1}] which was obtained
269 using breakthrough curves (BTCs) of tracer transport experiment. The HYDRUS 2D model
270 was used to solve governing equation for water flow and solute transport (Simunek et al. 1996).
271 A two dimensional numerical domain having similar dimension of sand tank was created to
272 simulate soil water flow and LNAPL transport through saturated zones. Thus, in this case S_f
273 i.e. fluid saturation in pore space [L^3L^{-3}] was taken as 1 as the media fully saturated. The
274 simulation domain was discretised in small grids of size 1 mm in a hexahedral geometry for
275 solving the governing equation numerically. The Galerkin finite elements method integrated
276 with Crank-Nicholson iterative scheme was used for the solution. The soil water flow and
277 solute transport parameters listed in table 1 were used as model input parameters. The hydraulic
278 behavior or parameters were obtained by inverse solution in HYDRUS 2D (Simunek et al.,
279 2012).

280

281 **3.1 Initial and boundary conditions**

282 The simulation domain was assigned no background concentration (zero) as initial solute
283 condition. The saturated moisture content was taken as the initial moisture level of the domain
284 and the top boundary was considered as the water table. Right side boundary (was taken as
285 continuous flux by incorporating respective pulse of influx for 1, 2, and 4 hours to maintain
286 groundwater table fluctuation along with base groundwater velocity. Similarly, left side
287 boundary was taken as a pulse out-flux for the respective cases. In case of stable groundwater
288 table condition, constant influx and out-flux was taken without pulse condition. No flux
289 condition was considered as the lower boundary condition. A LNAPL releasing point was
290 incorporated at same location as of two dimensional laboratory sand tank setup.

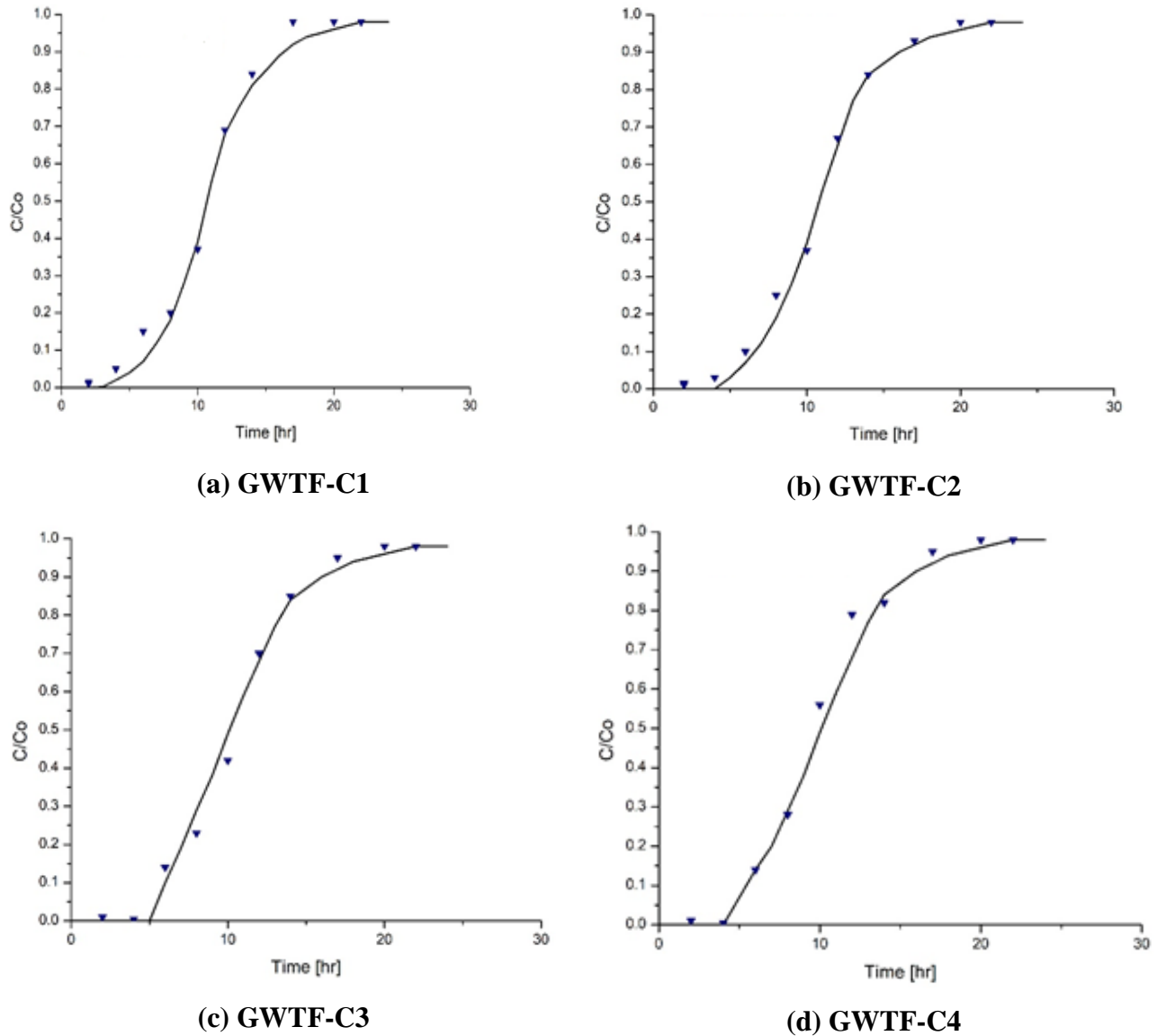
291

292 **4. Results and Discussion**

293

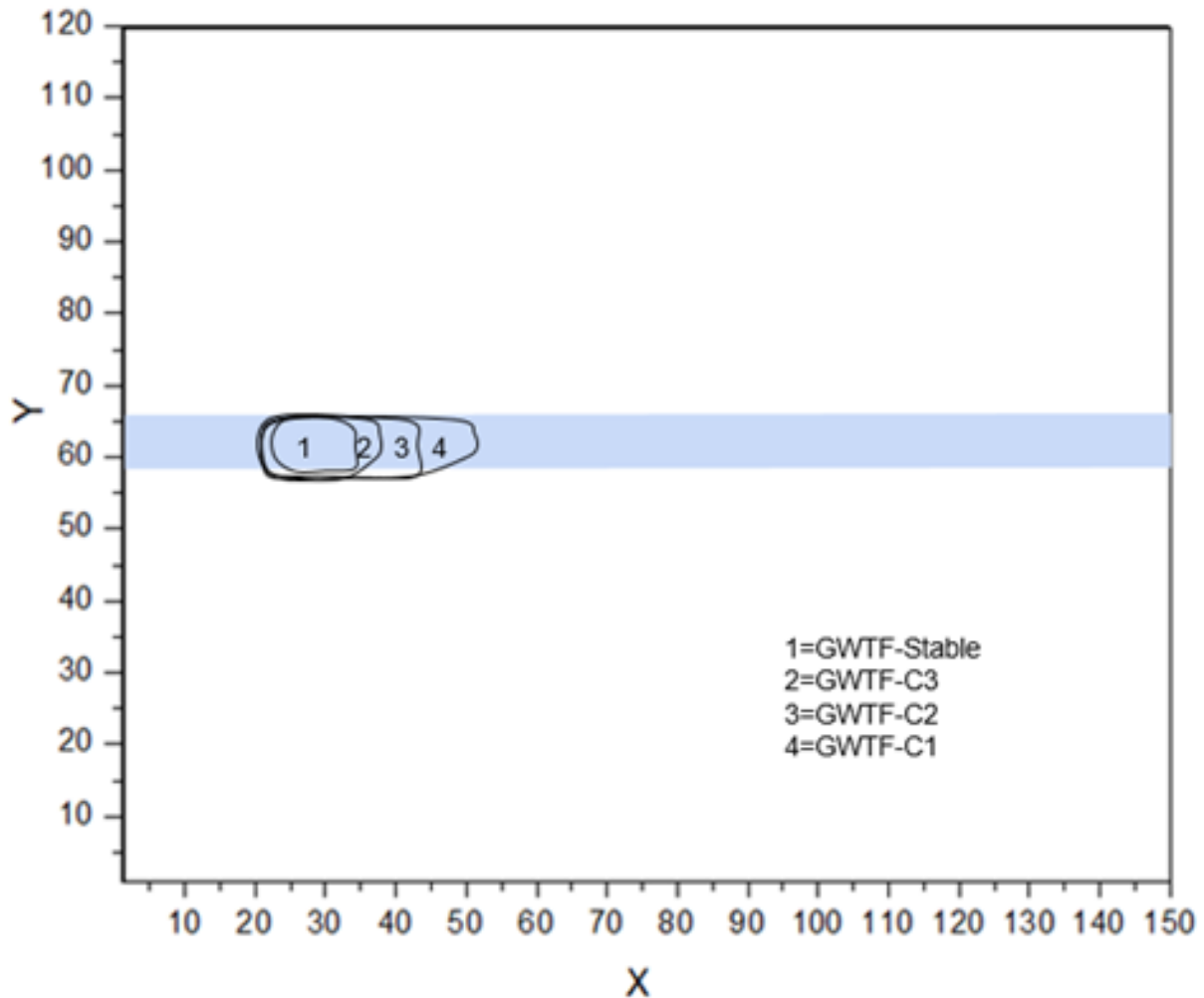
294 The breakthrough curves (BTCs) of tracer experiments under stable and different groundwater
295 fluctuation cases are presented in Figure 2 for rapid, general and slow groundwater table
296 fluctuation conditions represented as GWTF-C1, GWTF-C2, GWTF-C3, respectively. The
297 slope of the BTCs shown in Figure 2 are of similar trend, suggesting that the sand was packed
298 uniformly in each set of experiments without any significant preferential flow paths. The best
299 fit values of dispersion coefficient values are 0.000246, 0.0000171, 0.0000108, 0.0000073

300 m^2/s for rapid, general, slow, and stable groundwater table fluctuation conditions respectively.
 301 Similarly, estimated longitudinal dispersivity values are 1.23, 0.72, 0.28, 0.12m for rapid,
 302 general, slow, and stable groundwater table fluctuation conditions respectively. The observed
 303 values of dispersivity was used to simulate dissolved LNAPL plume in identified domain under
 304 corresponding groundwater table case.



305
 306
 307
 308
 309
 310

Figure 2: BTCs obtained from tracer test analysis for (a) rapid, (b) general, (c) slow and (d) stable groundwater fluctuation conditions.



311
312

313 Figure 3: Coverage of the LNAPL pool in smear zone subjected to different groundwater
314 fluctuation conditions.

315

316 **4.1 Pure phase LNAPL coverage and dissolution**

317 An effort has been made to capture LNAPL pool area in two dimensional sand tank
318 experiments under stable and fluctuating groundwater cases. For this purpose, periodically soil-
319 water samples were analyzed by GC-MS/IRMS technique (Dempster et al. 1997). The
320 interpreted boundary of pure phase LNAPL pool is presented in Figure 3 which shows a total
321 area of 250, 200, 160 and 70 cm² covered under rapid, general, slow and stable groundwater
322 fluctuation cases, respectively.

323 Experimentally observed area of pure phase LNAPL pool was used to determine the
324 characteristic length of the pool and for the estimation of dissolution rate. It can be
325 observed from the results that the rapid groundwater fluctuation causes the pure phase LNAPL
326 pool to spread over more area than the stable groundwater case. A high groundwater velocity

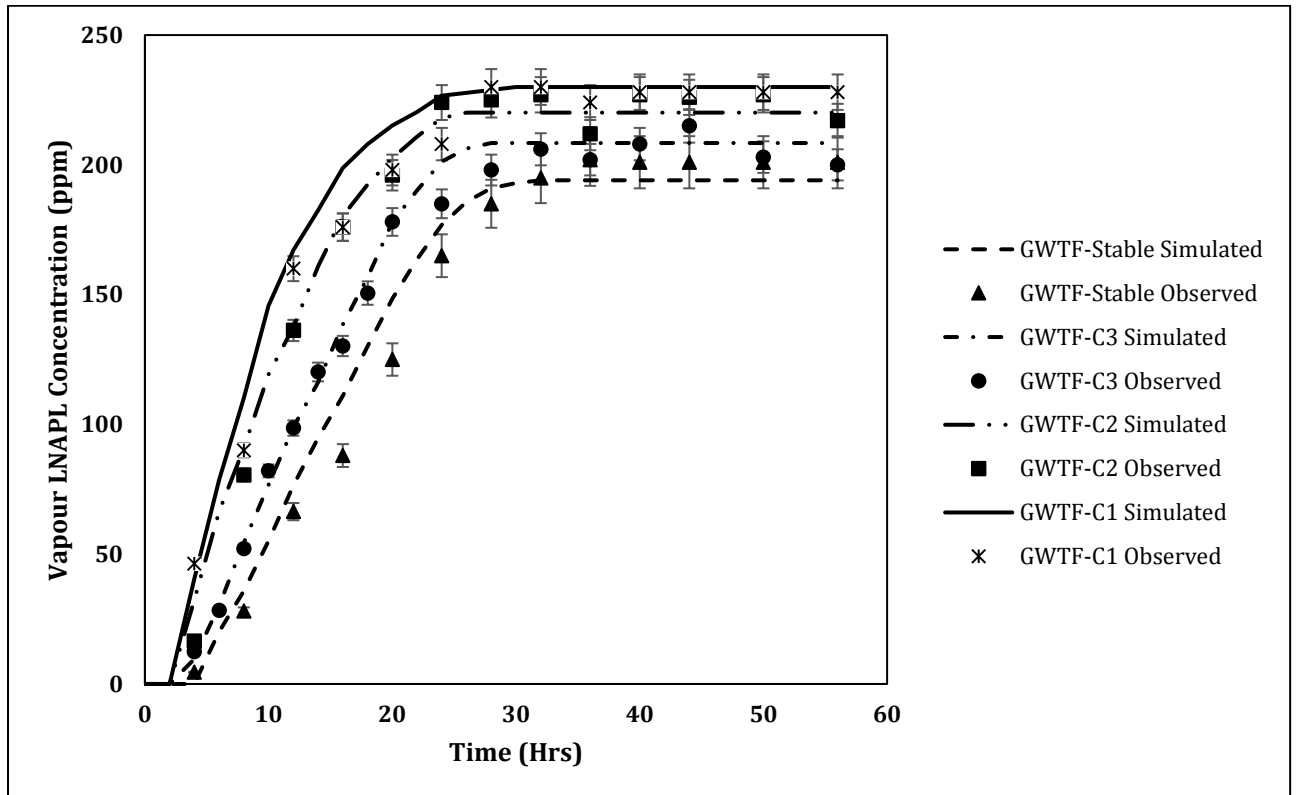
327 due to rapid fluctuation in groundwater governs the excess spreading of LNAPL in flow
328 directions. Spreading of pure phase LNAPL over a large area provides more dissolving surface
329 as LNAPL-water interphase to underlying flowing groundwater resulting into more dissolution
330 rates. Similarly, the large LNAPL pool contributes more LNAPL vapour to the overlying
331 unsaturated zone. Further, the volume of water contacting the LNAPL pool surface increases
332 as it spread in large area which also leads to high dissolution rates. This in turn significantly
333 increases dissolved phase concentration load to receiving groundwater and vapor
334 contamination to unsaturated pore air (Dobson et al. 2007; Vasudevan et al. 2014). On the other
335 hand, large coverage of pool contributes more LNAPL mass to capillary ganglia as smaller
336 blobs/fingering, which also play significant role in dissolution under rapid groundwater table
337 conditions. As noted by Sarikurt et al. (2017), the contact time and area of LNAPL-water
338 interphase is significant for dissolution rate and subsequent transport of dissolved LNAPL in
339 subsurface. Similarly, Sulaymon and Gzar (2011) highlighted that length of LNAPL-water
340 interphase plays important role to control the equilibrium concentration of dissolved LNAPL
341 plume. Results of this study confirm that the groundwater table fluctuation causes more
342 spreading of pure phase LNAPL pool itself which ultimately provide more LNAPL-water
343 dissolving area in smear zone. High dissolution rate from large LNAPL pool contributes high
344 concentration of dissolved LNAPL to the downgradient ports. The estimated LNAPL pool
345 coverage area under different cases can be used to forecast dissolved LNAPL plume under
346 dynamic groundwater flow conditions.

347

348 **4.2 Vapor phase concentrations**

349 The vapor phase LNAPL concentrations are plotted as BTC in Figure 4. The BTC shows a high
350 LNAPL concentration in case of rapid fluctuating groundwater table followed by general, slow
351 and stable groundwater table case. The vapor equilibrium concentration was observed as 210-
352 230 ppm in fluctuating condition while 180-185 ppm was observed in stable groundwater case.
353 This means a raising groundwater table carries pure phase LNAPL mass upward and a falling
354 groundwater allows LNAPL to move downward. During dynamics of groundwater level, the
355 trapped LNAPL remain behind in smear zone which creates a large interphase area of air-
356 LNAPL/water (Powers et al. 1992). Therefore, more vapor phase concentration was observed
357 from the residual LNAPL. These results are in line with the findings of study conducted by
358 Oostrom et al. (2006) with 2D experiments under water table dynamic conditions. The study
359 found a considerable residual LNAPL saturation in smear zone. The high vapor concentration
360 can also be attributed to the partition of LNAPL from large dissolved phase plume having high

361 concentration. Further, lowering of groundwater table increases air-filled porosity in smear
 362 zone, which eventually affects vapor phase LNAPL partition. The BTC of different
 363 groundwater table fluctuation experiments confirms that the vapor intrusion is highly
 364 dependent on the nature of groundwater table conditions (Patterson and Davis, 2009). High
 365 vapor LNAPL in unsaturated pores may become toxic for the indigenous microorganisms.
 366
 367



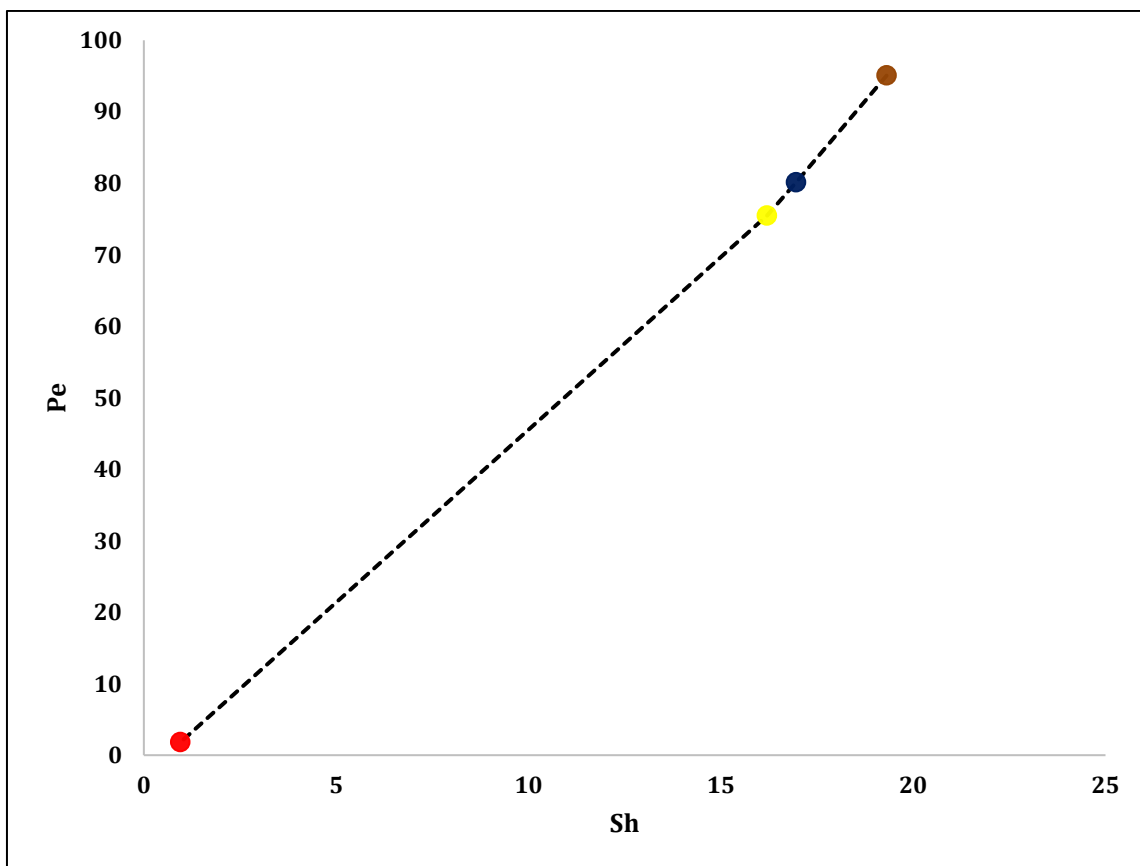
368
 369
 370 Figure 4: BTC representing LNAPL concentration in soil air in 2D sand tank under stable and
 371 fluctuation groundwater table conditions.

372
 373 The measured pure phase LNAPL pool area was used to estimate its characteristic length of
 374 LNAPL pool ($l_{(c)}$) under stable and fluctuating groundwater conditions. The observed values
 375 of $l_{(c)}$ was found 15.81, 14.15, 12.64, and 8.36 cm under rapid, general, slow and stable
 376 groundwater fluctuation conditions, respectively. The estimated value of mass transfer
 377 coefficient (k^*) are listed in Table 3. The estimated Sherwood numbers (Sh) were found 0.95,
 378 16.20, 16.95 and 19.30 while Peclet numbers (P_e) were 1.80, 75.47, 80.14, and 95.06 for rapid,
 379 general, slow and stable cases respectively. A high value of Sh indicates that dissolution was
 380 a dominating process under fluctuating groundwater conditions. The reason for high Sh can be

381 attributed to the large pool spreading, which provides more LNAPL-water interphase under
382 fluctuating groundwater condition. Further, more contact time of underlying groundwater with
383 the large dissolving LNAPL pool also accelerate the dissolution rate. Likewise, high P_e
384 indicates that the advective flow was dominant than the diffusive flow under fluctuating
385 groundwater conditions. However, one cannot ignore the importance of diffusive flux under
386 stable groundwater flow regimes. The correlation Sh with P_e is presented in Figure 5 with the
387 coefficient of determination (R^2) value of 0.998. This kind of high correlation between Sh and
388 P_e was also reported in a recent study by Sarikurt et al. (2017).

389

390



391

392 Figure 5: Correlation between Sh and P_e . Red, yellow, blue and green circle represent

393 stable, slow, general and rapid groundwater fluctuation conditions respectively.

394

395

396

397

398 Table 3: Estimated values of k^* and corresponding values of Sh and P_e under dynamic
 399 groundwater table conditions

Conditions	Mass transfer coefficient k^* (m/s)	Sherwood Number Sh (-)	Peclet Number P_e (-)
GWTF-C1	9.50E-02	19.30	95.06
GWTF-C2	5.80E-03	16.95	80.14
GWTF-C3	3.50E-03	16.20	75.47
GWTF-Stable	1.20E-04	0.95	1.80

400

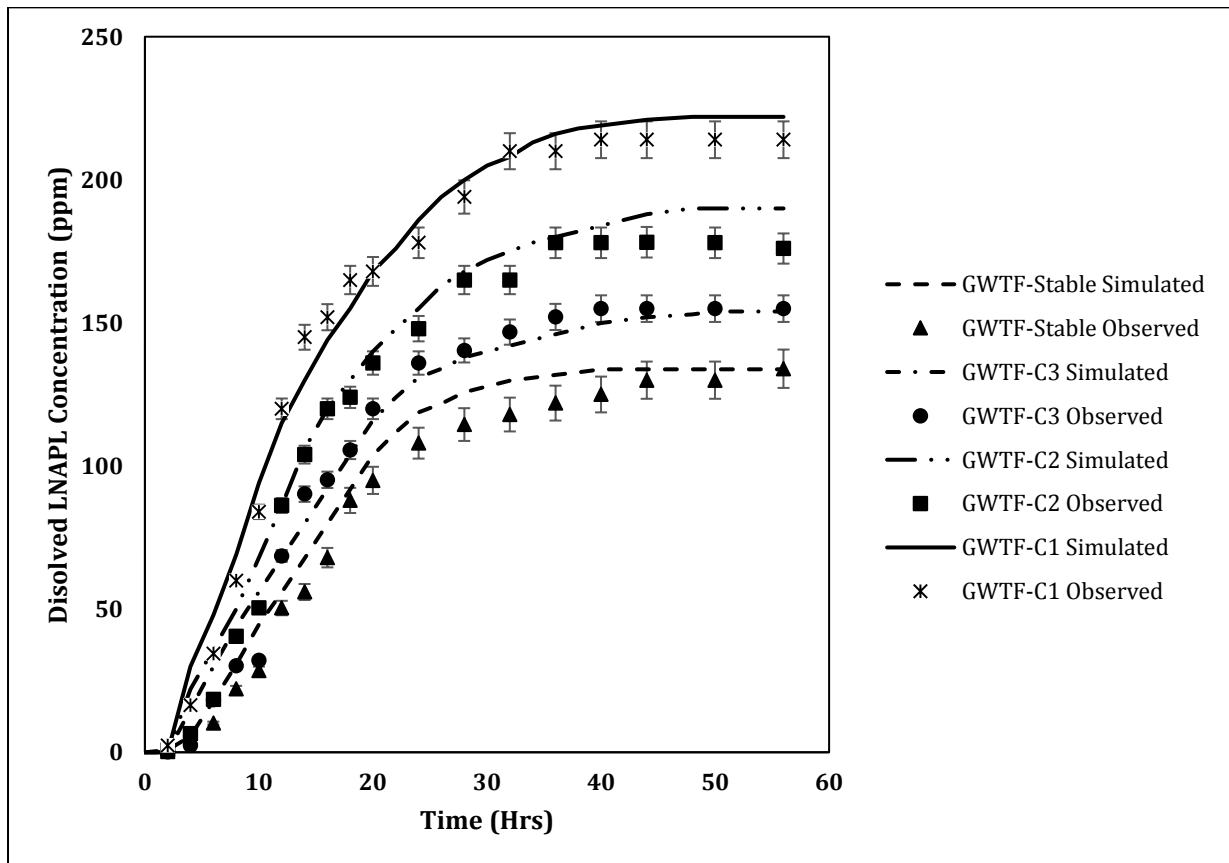
401 4.3 Dissolved phase concentrations

402 Dissolved LNAPL concentrations as a function of time for all four cases are presented in
 403 figures 6-7. In figure 6a, BTC is presented for port 1 (top sampling layer: X:25cm; Y:60 cm)
 404 which was situated just below the water table and nearby LNAPL pool. It shows that toluene
 405 concentration starts rising after few hours and increases rapidly and then starts attenuating
 406 before reaching to a concentration of 200-230 ppm for rapid fluctuating groundwater case.
 407 Similar trends were observed for the remaining fluctuating groundwater cases. The higher
 408 concentration in the rapid fluctuation case was due to more dissolving LNAPL pool area than
 409 general, followed by slow and stable fluctuation conditions. Likewise, BTCs of port 4 and port
 410 7 of upper layer are presented in figure 6b and 6c respectively. LNAPL concentration takes 10-
 411 12 hours and 20-26 hours to reach port 4 and port 7, which was 55 cm and 115 cm away from
 412 pool respectively. However, a significant difference in the final equilibrium concentration
 413 (plateau) was observed amongst different groundwater table fluctuation cases. At this stage the
 414 supply from the source and the out flux at the observed down-gradient port (port 7) was
 415 reaching to an equilibrium condition. A decreasing trend in the equilibrium concentration was
 416 observed as plume moves from up gradient location (port 1) to down-gradient locations (Port
 417 4/7) which represents the dependency of biodegradation rate on dissolved LNAPL
 418 concentration. In general, the equilibrium concentration of toluene in earlier studies was found
 419 quite nearby to its dissolution limit. In this study, the observed concentration of toluene was
 420 not able to reach the maximum solubility value of toluene because of (a) limited contact (water-
 421 toluene) time of opportunity, (b) the concurrent biodegradation of the dissolved LNAPL in
 422 sand tank setup. The study shows that more than 150 ppm dissolved LNAPL concentration was
 423 found to start inhibiting metabolic actions of microbes causing lower degradation rates then its

424 potential rate. Similarly, a concentration less than 100 ppm provides insufficient carbon sources
 425 to microbes resulting in comparatively low biodegradation rate of toluene. The optimal
 426 biodegradation rate was found in plume area having concentrations ranges from 120-150 ppm,
 427 especially under general groundwater condition. While biodegradation rate become quite slow
 428 at port 1 due to high dissolved LNAPL concentration (>150 ppm) and causes toxicity to
 429 potential microbes. The biodegradation rate in upper layer was accelerated by high diffusion
 430 of oxygen from head space by fluctuating groundwater table.

431 Likewise, the dissolved LNAPL concentrations are presented in figures 7a-c for ports
 432 8, 11 and 14 situated in bottom layer. Figure 7a shows that the dissolved LNAPL plume takes
 433 10-12 hours to reach at port 8, which is at 30 cm downward from the pool. At port 8, there is
 434 very less difference in equilibrium concentrations as compared to port 1. Whereas, a large
 435 difference was found in equilibrium concentration of port 11 (Figure 7b) and port 14 (Figure
 436 7c) in comparison to port 8 (Figure 7a). This seems due to high biodegradation rates at port 11
 437 as compared to port 8, even the port 11 is situated in bottom layers where background oxygen
 438 level is low.

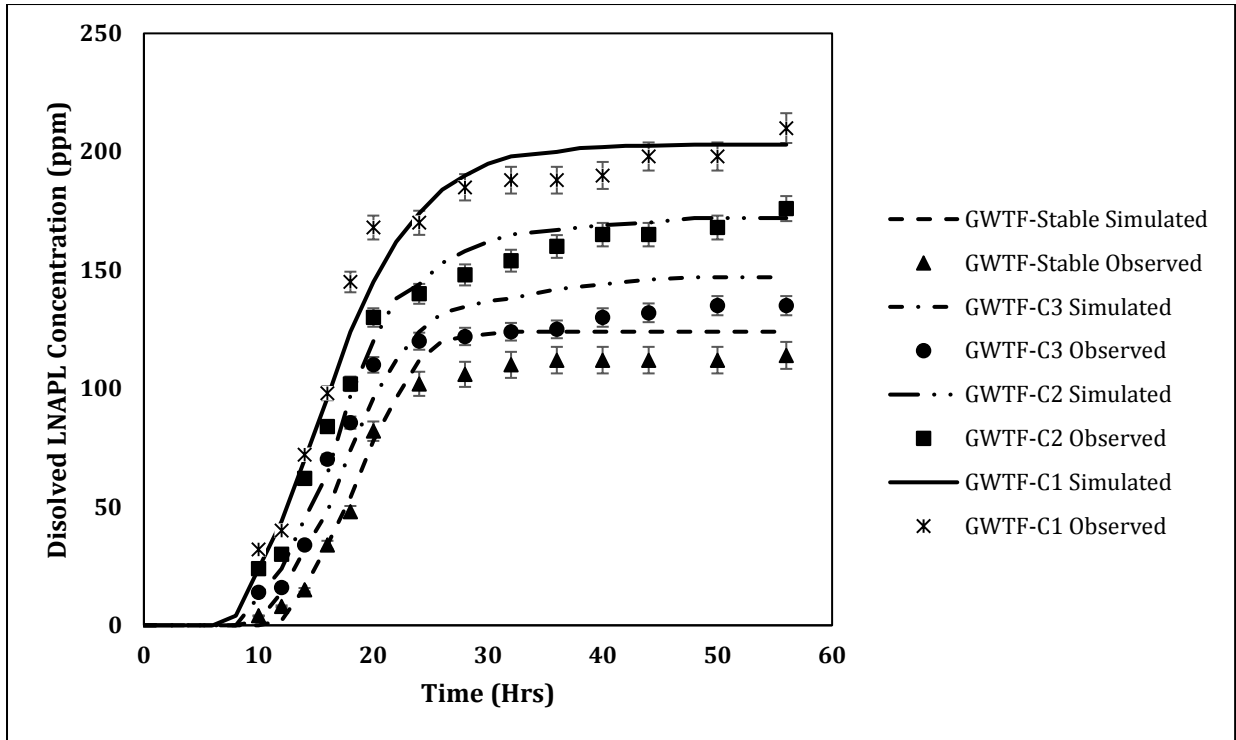
439



440

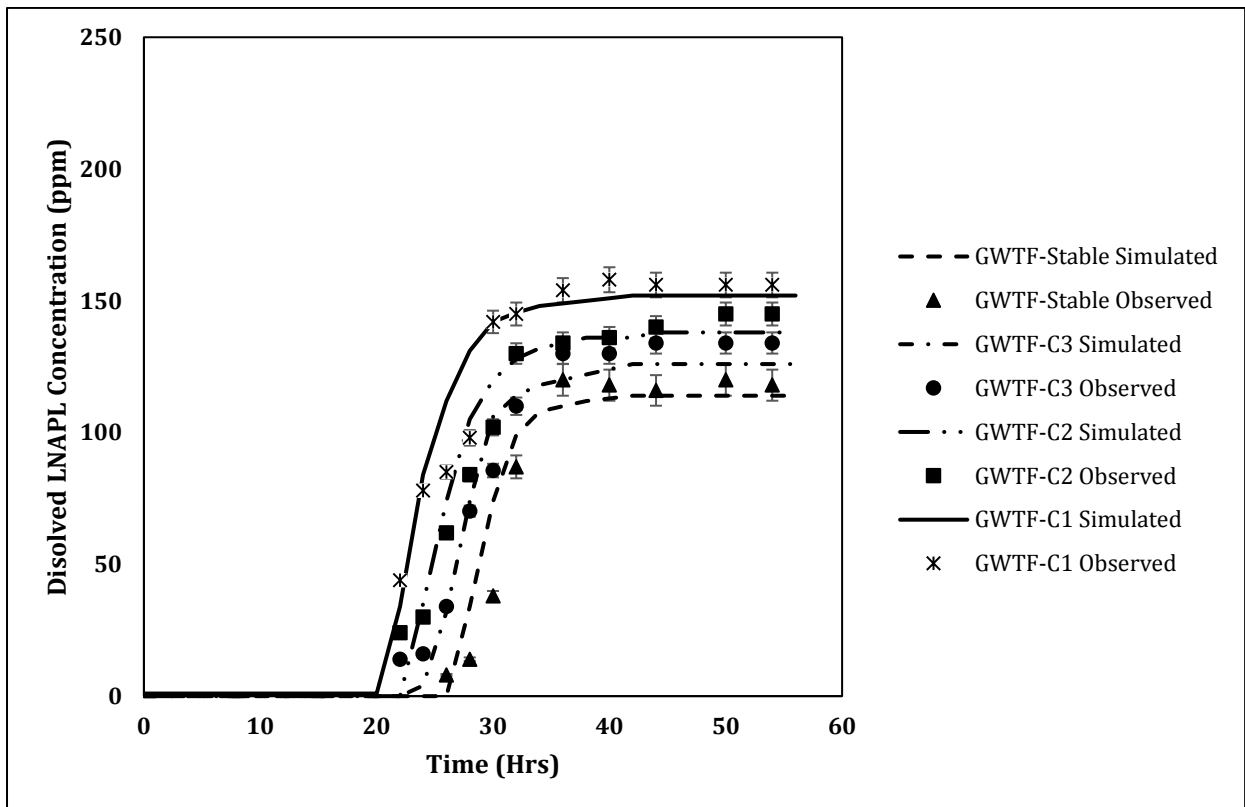
441

(a) Port 1: X:25; Y:60



442
443
444

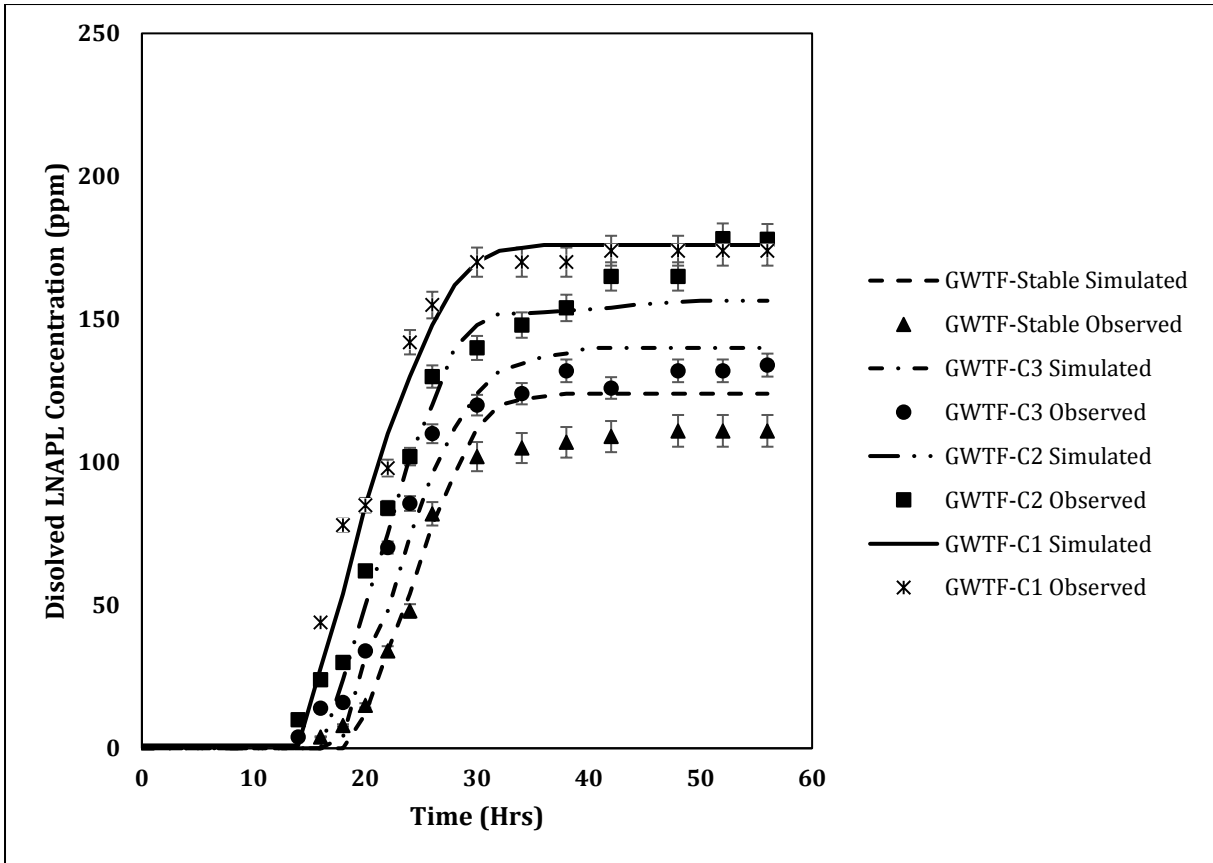
(b) Port 4: X:80; Y60



445
446
447
448

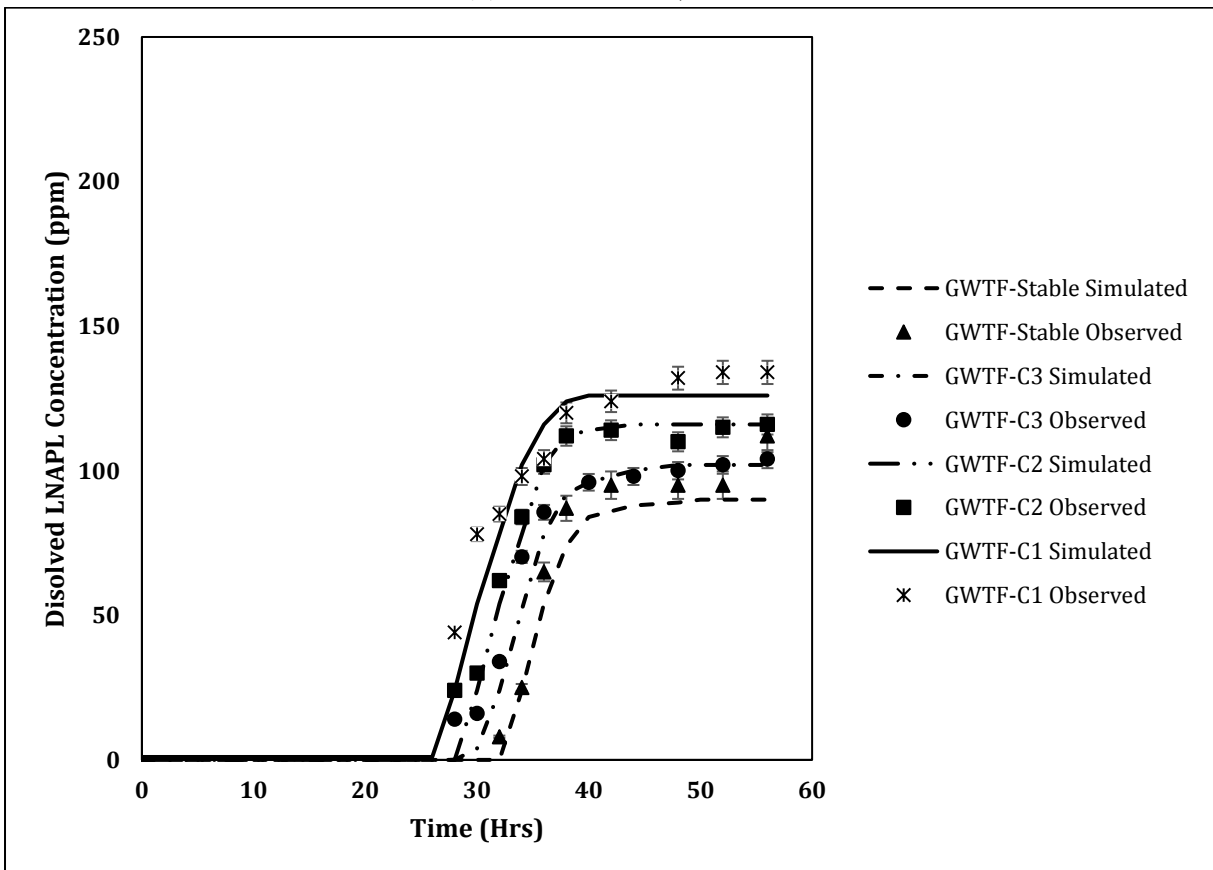
(c) Port 7: X:140; Y60

Figure 6: BTCs of (a) port 1, (b) port 4 and (c) port 7 under stable and fluctuating groundwater table conditions.



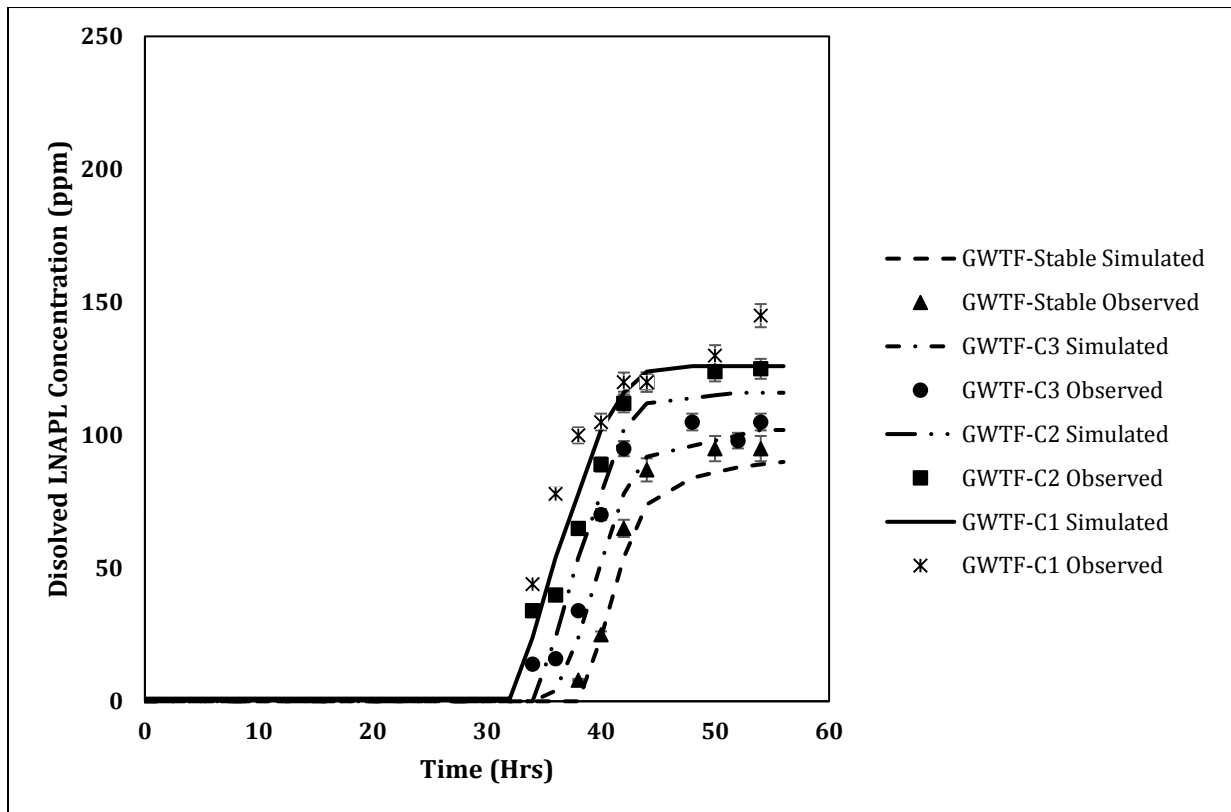
449
450

(a) Port 8: X:25; Y30



451
452
453

(b) Port 11: X:80; Y30



(c) Port 14: X:140; Y30

Figure 7: BTCs of (a) port 8, (b) port 11 and (c) port 14 under stable and fluctuating groundwater table conditions.

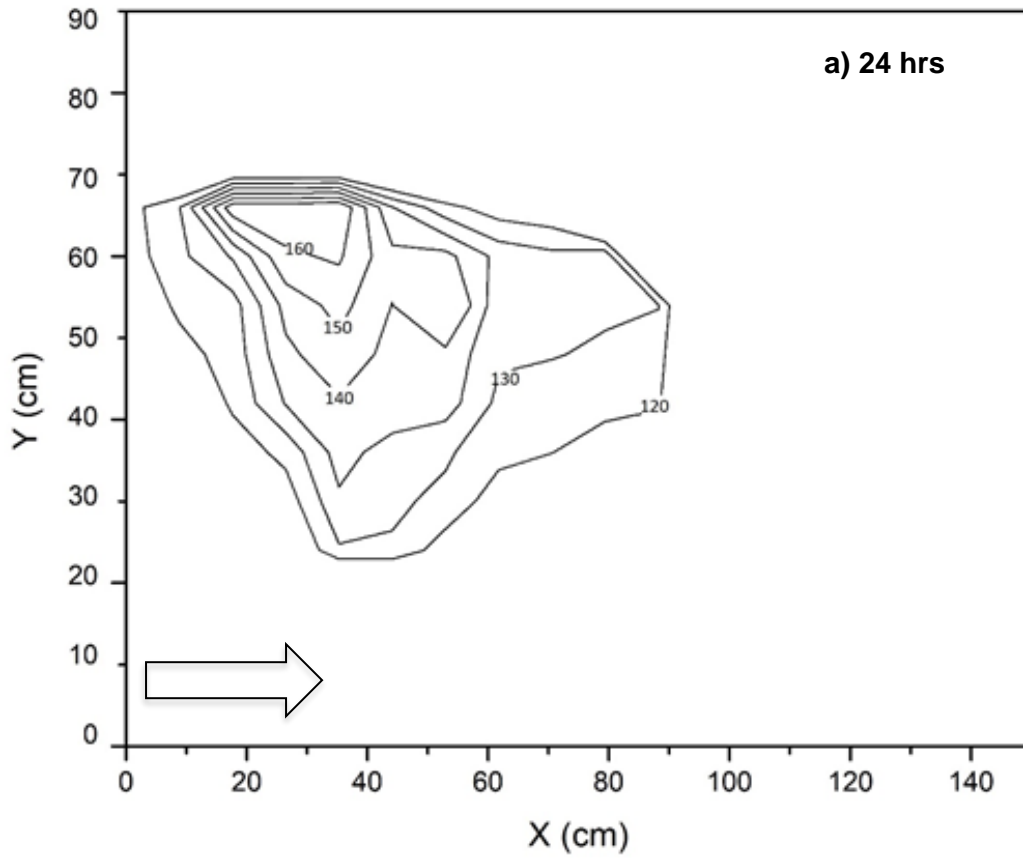
454
455
456
457
458
459
460
461
462
463
464
465
466
467
468
469
470
471
472
473

The experimentally observed dissolved LNAPL concentrations isolines are plotted as a function of space in figures 8a-d. These concentration isolines were plotted using experimentally measured data from all sampling ports (port1-14) including ports situated opposite to flow directions (port RP1-RP2). The objective of these isolines plot is to present different concentration zone originated from LNAPL pool under different selected groundwater table conditions. Figure 8a represents concentration isolines originated from large LNAPL pool having 15.81 cm under rapid groundwater table fluctuation condition. Thus, large dissolved plume was created with a concentration ranges from 120-160 ppm in initial 12 hours and later reaches up to 200 ppm nearby the pool location. A large area covered by high concentration i.e. greater than 150 ppm causes toxicity to potential microbes and thus low biodegradation rate was observed in this case. Thus, a closely spaced isolines were observed in rapid fluctuating groundwater conditions. Whereas, figure 8b represented isolines of dissolved plume originated from a pure phase LNAPL pool of characteristic length of 14.15 cm under general groundwater table fluctuation condition. In this case, the dissolved plume

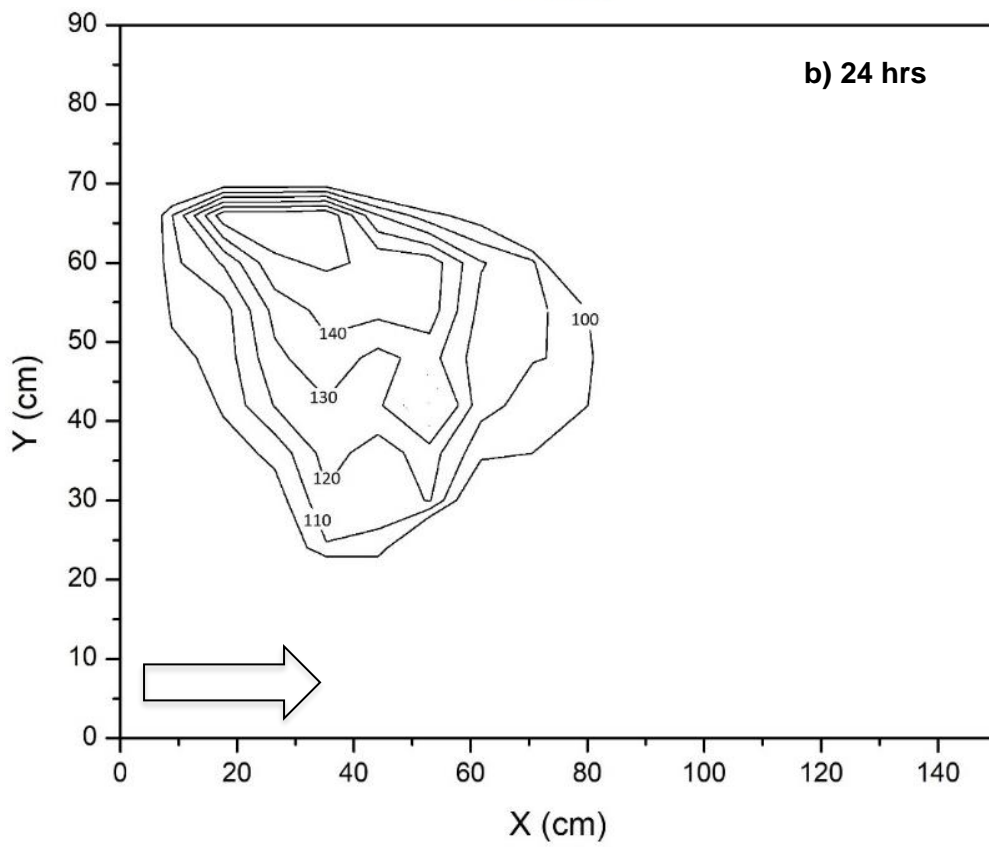
474 concentration ranges 110 ppm-140 ppm in initial 12 hours and continuously increases upto 160
475 ppm. Less concentration (20ppm) of dissolved plume under general groundwater table
476 fluctuation condition was due to smaller LNAPL pool length then the rapid case. Thus, in
477 general groundwater table fluctuation case, a large area covered by 130-150ppm concentration
478 LNAPL plume become carbon source to potential microbes and causes enhanced
479 biodegradation rates. Similar trends were observed in case of slow groundwater table
480 fluctuation condition as presented in figure 8c. While, comparatively small dissolved LNAPL
481 plume (figure 8d) having less concentration (i.e. range of 70 ppm-100 ppm in initial 12 hours
482 and 80-120 ppm in 56 hours) was observed in case of stable groundwater case.

483 In this study, the concentration isolines clearly show the fast transport of dissolved
484 plume in horizontal direction than its transverse movement under stable and fluctuating
485 groundwater conditions. The horizontal spreading of plume was due to advection dominated
486 flow of the dissolved toluene originating from large contact area between LNAPL pool and
487 water. Dissolved LNAPL plume movement in opposite direction of groundwater flow driven
488 by diffusive flux is comparative very slow. Whereas, the expansion of dissolved LNAPL plume
489 in the vertical direction under fluctuating groundwater shows the crucial role of dispersive flux.
490 The diffusive flux of the dissolved LNAPL can play a crucial role in LNAPL movement under
491 stable groundwater regimes.

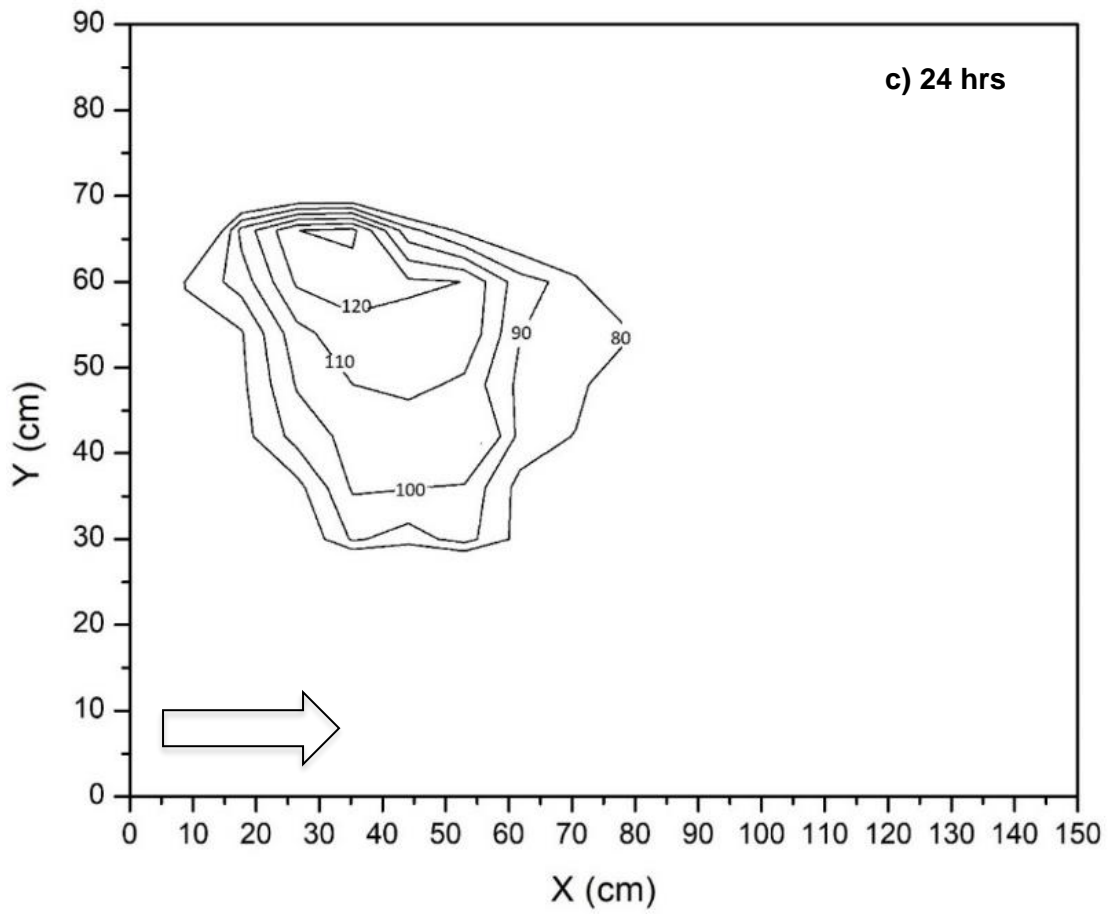
492



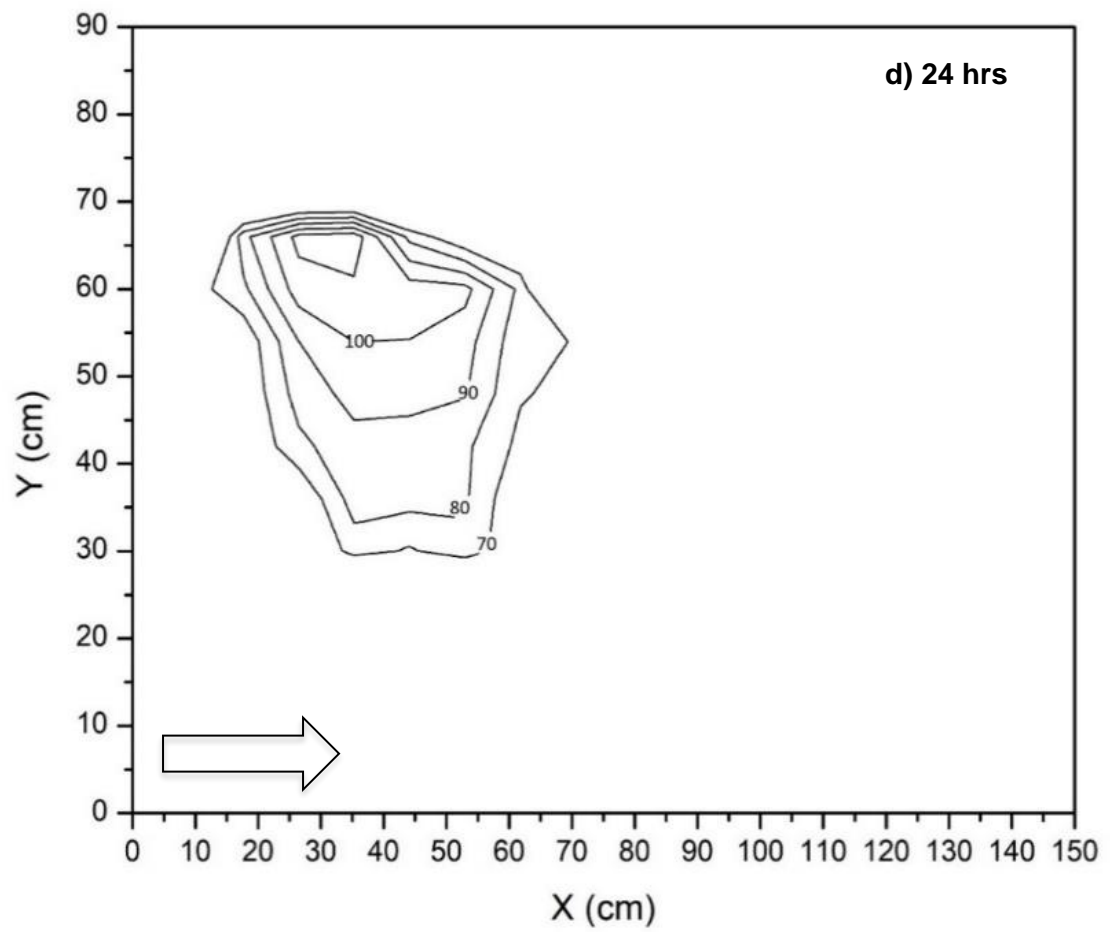
493



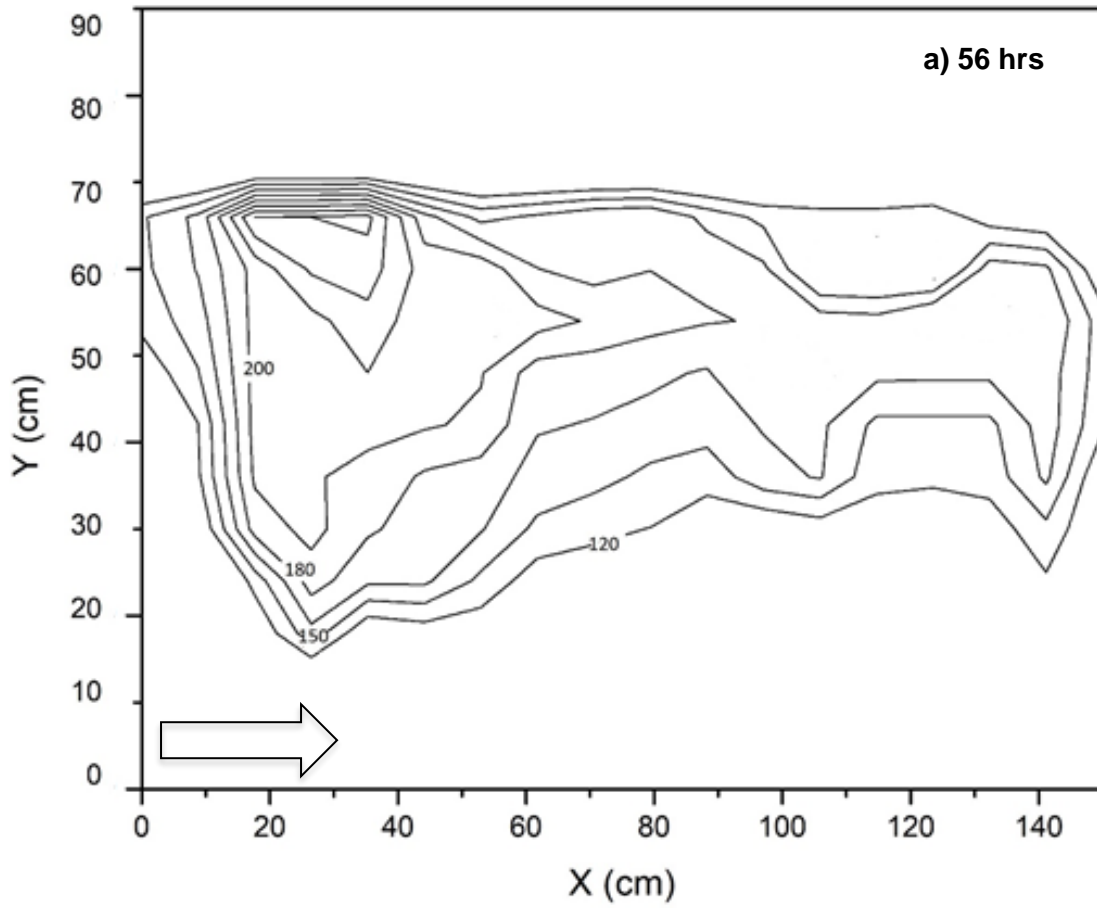
494



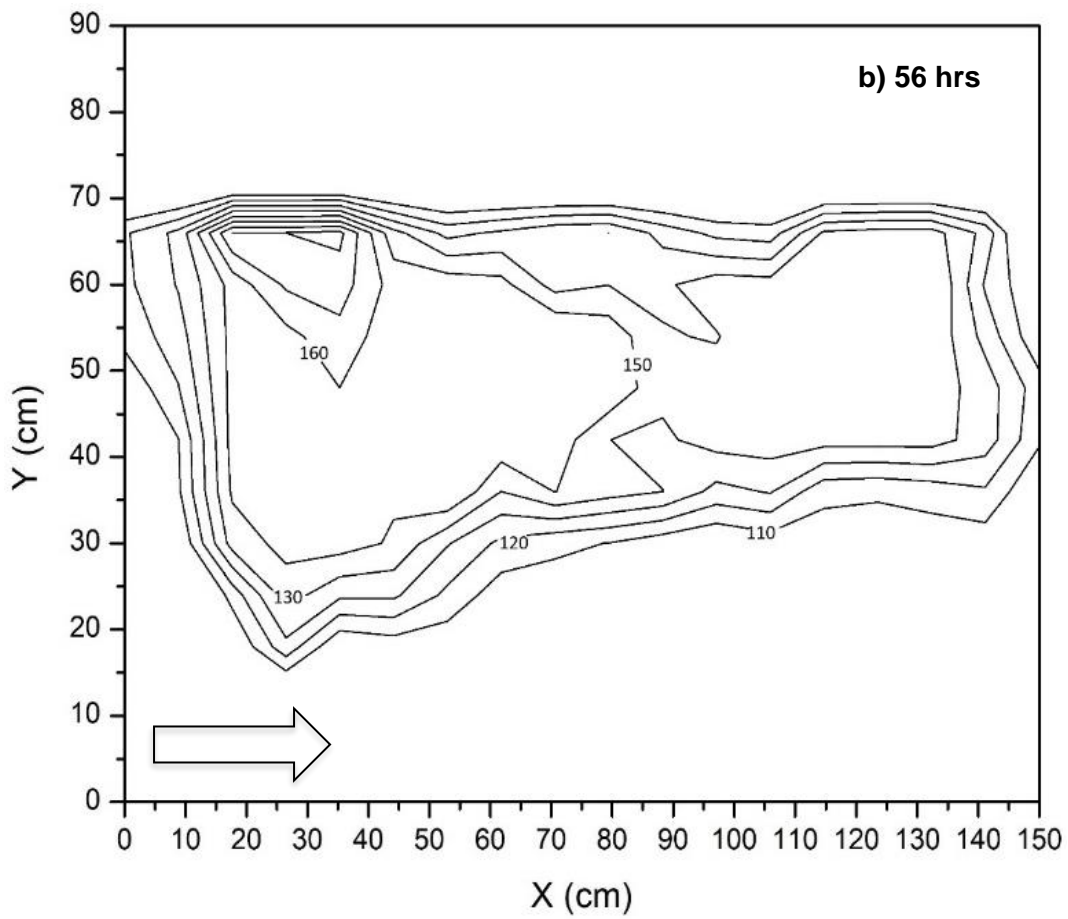
495



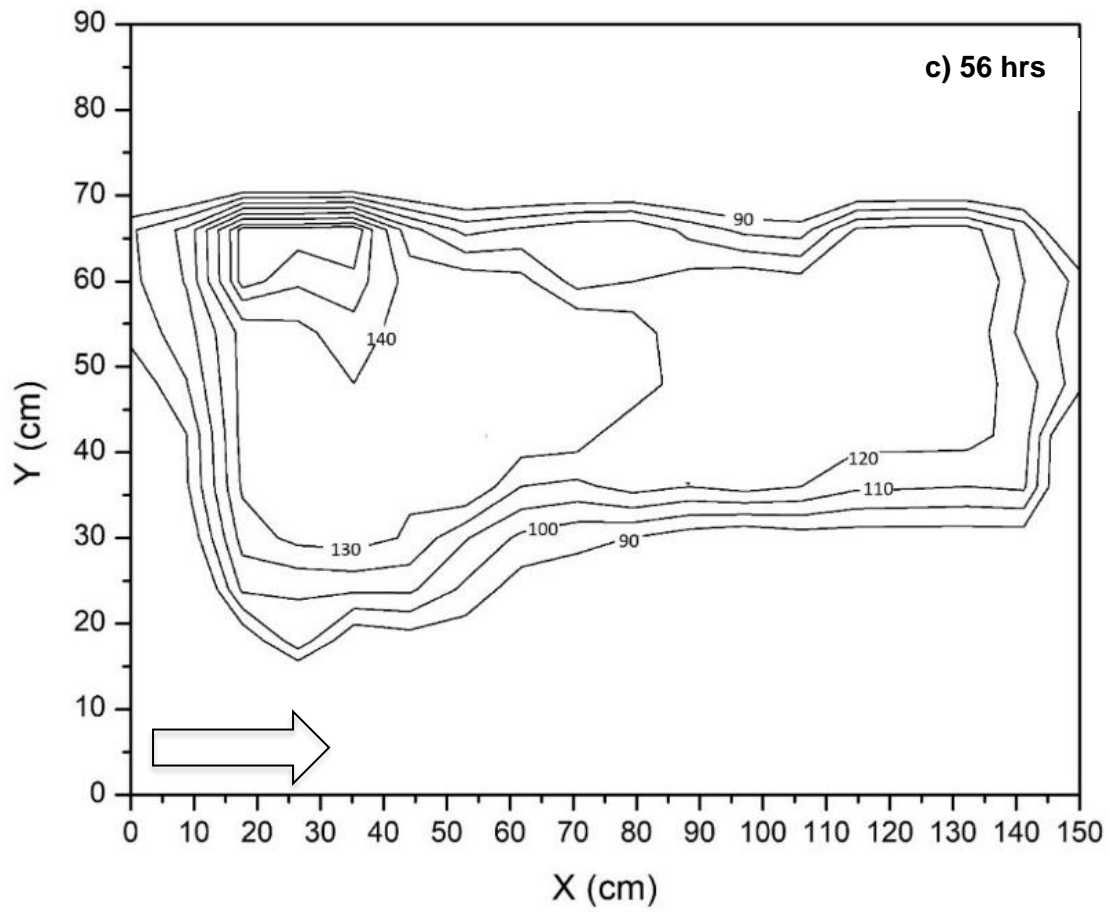
496



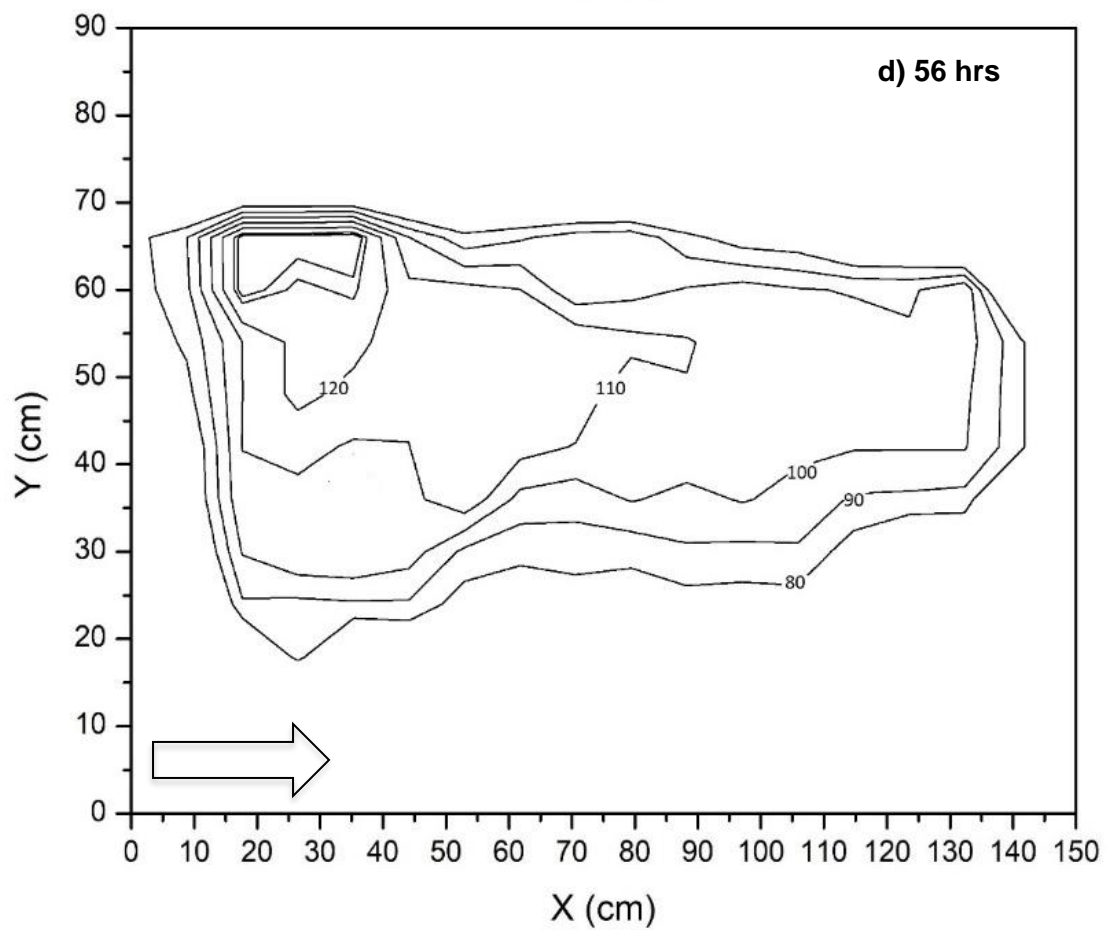
497



498



499



500

501 Figure 8: Concentration isolines presenting the extension of dissolved LNAPL plume
502 originated from pure phase source under a) rapid, b) general, c) slow and d) stable
503 groundwater table fluctuation cases.
504

505 **4.4 Biodegradation under different groundwater table fluctuation conditions**

506 Biodegradation rate of dissolved LNAPL plume originated from pooled LNAPL under stable
507 and fluctuating groundwater conditions was also investigated. For this purpose, spatial
508 biodegradation rates were estimated for port 1 and port 4 of upper sampling layer and port 8
509 and 14 of lower sampling layer. In Figure 9, the biodegradation rates were estimated using
510 corresponding values of equilibrium concentration of upward port and subsequent downward
511 port. Figure 9a presents biodegradation rate of port 4 situated 55 cm away from LNAPL pool.
512 At this location, biodegradation rates of 0.5 ppm/hour, 0.55 ppm/hour, 0.26 ppm/hour, and 0.13
513 ppm/hour were observed for dissolved LNAPL zone with the concentration of 180 ppm, 150
514 ppm, 120 ppm, and 100 ppm under rapid, general, slow and stable groundwater table condition,
515 respectively.

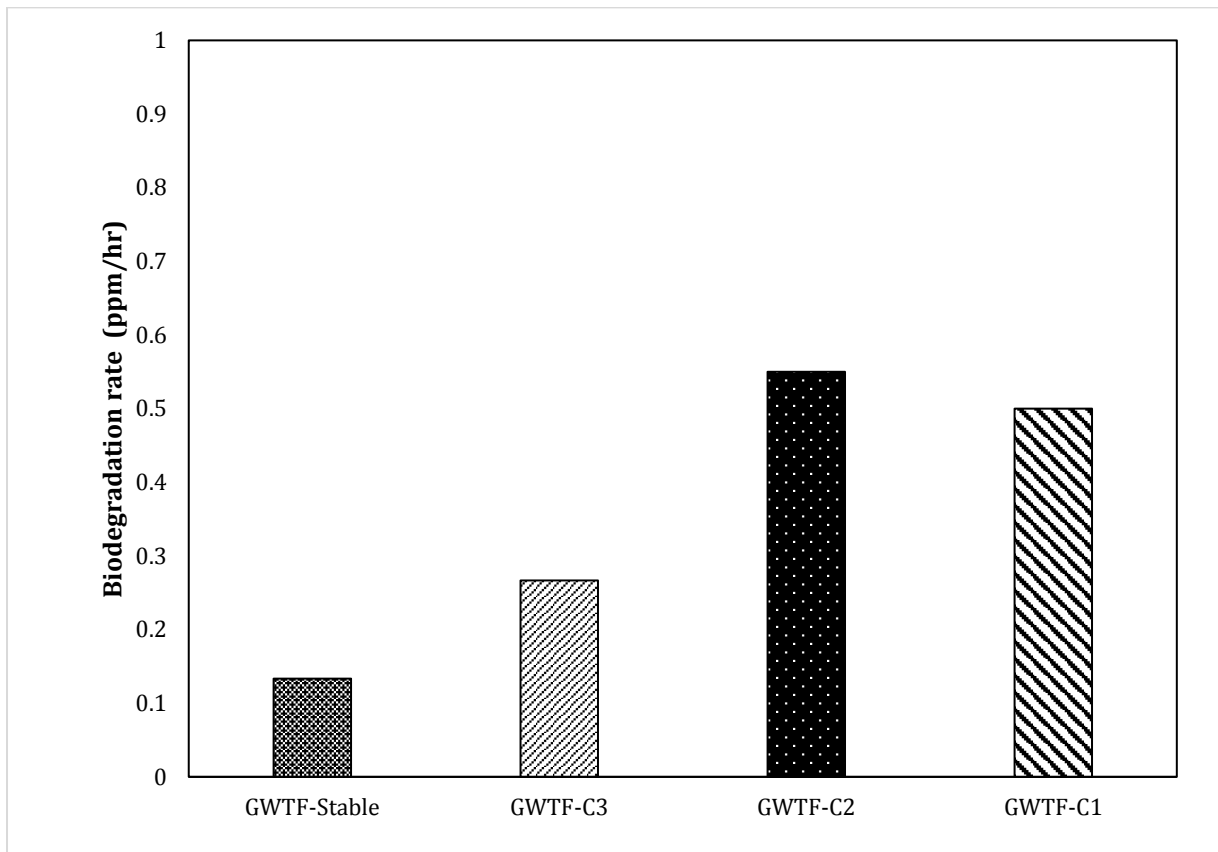
516 The biodegradation rate was found comparatively low in case of rapid fluctuation than general
517 fluctuation because of large high concentration (>150 ppm) region which causes toxic effects
518 on potential microbes lies in this region. While, the high biodegradation rate in case of general
519 than slow and stable groundwater fluctuation conditions proves the dependency of microbes
520 on dissolved LNAPL concentrations. Figure 9b represents biodegradation rates for port 7 of
521 upper layer having dissolved LNAPL concentration in the range of 100 ppm-150 ppm.
522 Similarly, Figure 9c and 9d shows the biodegradation rates for port 8 and port 14 of lower layer
523 respectively. Comparatively low biodegradation rates were observed in lower layer ports under
524 stable groundwater conditions, even if the dissolved LNAPL concentration was in the optimum
525 range of 100 ppm-150 ppm. These low biodegradation rate at lower ports was due to
526 comparatively less populated potential microbes due to low oxygen level. While, the
527 biodegradation rates were also increases at lower port in case of fluctuating groundwater
528 conditions. These accelerated biodegradation rate can attribute to the fact that the additional
529 oxygen to background level was added due to fluctuation in water table, which enhance the
530 microbial growth.

531 Microbial population was also counted using standard plate count method for periodically
532 collected soil-water samples from port 1 and port 7 of upper layer and port 8 and port 14 of
533 lower layer. The estimated CFU of collected soil-water samples were listed in table 4.
534 Initially, microbial count of $216.2-258 \times 10^4$ CFU/mL and $142.5-147.2 \times 10^4$ CFU/mL was

535 observed at upper and lower layer respectively. In GWTF-C1 case, the microbial count at port
536 1 increases upto 305×10^4 CFU/mL in 24 hours and then decreases to 78×10^4 CFU/mL in 56
537 hours. Similarly, at port 7, overgrowth was recorded after 24 hours thereafter decreases to
538 224×10^4 CFU/mL in 56 hours.

539 The enhanced microbial growth was observed as dissolved LNAPL concentration
540 reached around 140-150 ppm at this location which provides sufficient carbon source to
541 microbes. However, when the dissolved LNAPL concentration reaches higher than 150 ppm,
542 it become toxic to microbial community. Increasing microbial count was recorded at both port
543 of top layer due to optimum dissolved LNAPL concentration and sufficient oxygen level in
544 general and slow groundwater fluctuation. Microbial count was recorded very low at port 14
545 of lower layer due to low concentration of dissolved LNAPL and insufficient oxygen level
546 under all groundwater table conditions. Growing population of the microbial community at
547 petroleum hydrocarbon-contaminated groundwater observed due to seasonal groundwater level
548 fluctuations by Zhou et al. (2015). Such microbial analysis may help to implement nutrient and
549 or electron acceptor plan to enhance petrochemical degrading microbes.

550



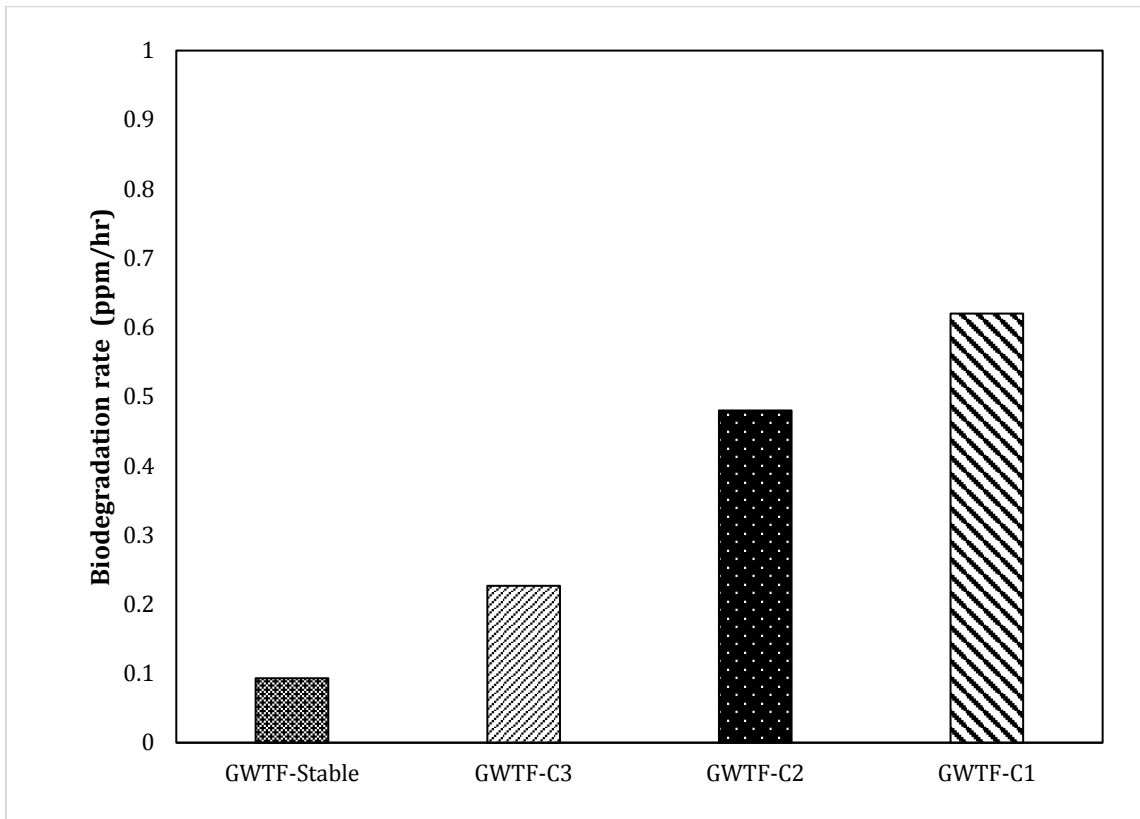
551

552

553

(a)

554

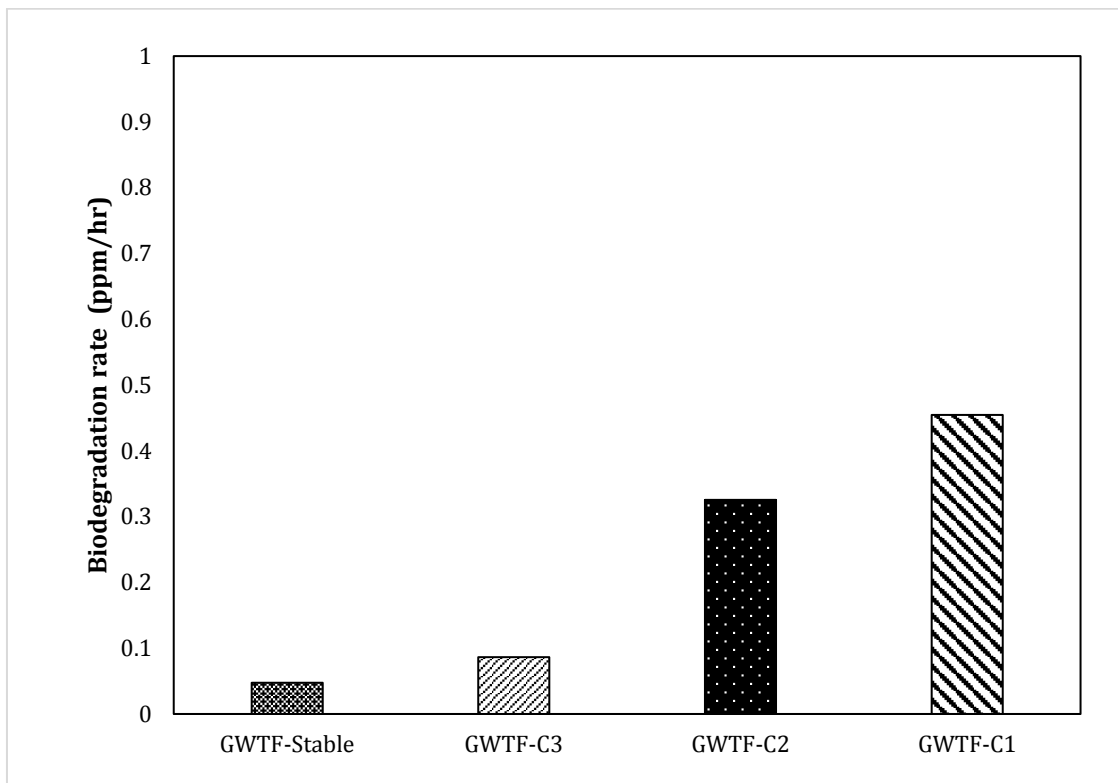


555

556

557

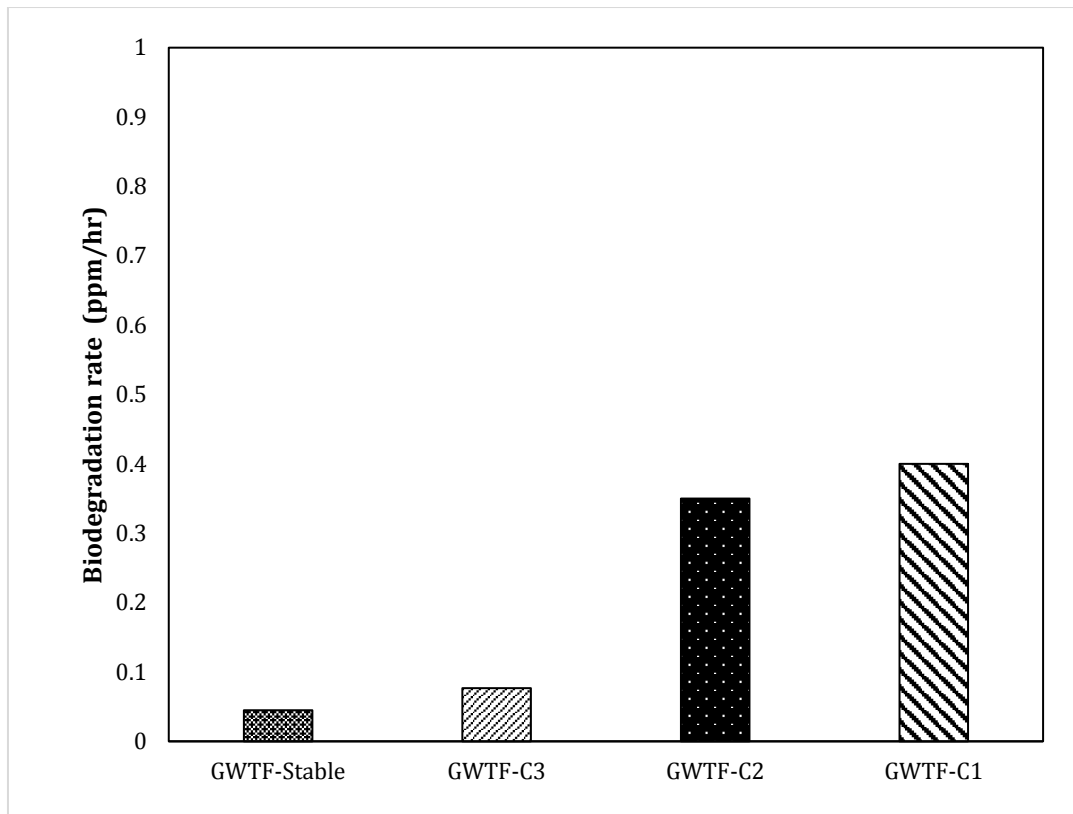
(b)



558

559

(c)



(d)

560

561

562

563 Figure 9: Biodegradation rates under stable and fluctuating groundwater conditions observed
 564 at (a) port 1 and (b) port 7 of upper sampling layer and (c) port 8 and (d) port 14 of bottom
 565 sampling layer of 2D sand tank setup.

566

567 Table 4. Microbial population count of samples collected from the experimental setup under
 568 different groundwater table conditions.

569

Condition	Port 1			Port 7			Port 8			Port 14		
	10 ⁴ CFU/mL			10 ⁴ CFU/mL			10 ⁴ CFU/mL			10 ⁴ CFU/mL		
	0hr	24hr	48hr									
GWFT-C1	254.5	305	78	258.0	O	224.5	147.2	165	135.4	142.5	145.8	165
GWFT-C2	232.1	294.8	304.6	-	285.0	O	145	174.2	235.0	-	164.5	218
GWTF-C3	216.2	285.4	277.5	224.5	288.0	O	144.5	210.5	270.6	-	164.2	235.6

570 O= Overgrowth

571

572

573

574 **5. Conclusion**

575 In this study, a series of laboratory experiments and numerical modelling was performed to
576 investigate fate and transport of LNAPL originated from pure phase LNAPL pool under stable
577 and fluctuating groundwater conditions. Three different groundwater fluctuating
578 experiments representing rapid, general and slow groundwater table fluctuation scenarios
579 were conducted by raising/falling water table by 5cm of magnitude in 1, 2, and 4 hours
580 respectively. Estimated pool area shows a large pure phase LNAPL pool in smear zone
581 under fluctuating groundwater conditions, resulting in accelerating dissolution rate from
582 large LNAPL-water interphase area. Simulated and observed BTCs show high dissolved
583 LNAPL concentration and large plume originated from large LNAPL-water interphase area
584 under rapid groundwater fluctuation condition. The time of arrival of plume shows that
585 transport of dissolved LNAPL was comparatively more in case of rapid fluctuating
586 groundwater condition. A high biodegradation rate was observed in regions having
587 concentration ranges from 140-160 ppm of dissolved LNAPL. While, low biodegradation rates
588 were observed for low dissolved LNAPL concentrations (<140 ppm) and also high
589 concentrations (>160ppm) which fortifies the dependency on initial dissolved LNAPL
590 concentrations. Further, microbial growth was found to be increasing as plume moves away
591 from the LNAPL pool, which shows detrimental impact of high concentration of toluene on
592 survival of indigenous microorganisms. Overall, this study suggest that groundwater table
593 fluctuations significantly affects the distribution, transport, and biodegradation of the LNAPL
594 contaminants in subsurface. The results of this study may be improved by considering
595 subsurface heterogeneity and fractures. This study may help in design, establishment and
596 implementation of bioremediation techniques to decontaminate LNAPL polluted sites,
597 especially under varying subsurface conditions.

598

599 **Acknowledgment**

600

601 The authors are thankful to the Department of Science and Technology (DST), India for
602 funding this research under the scheme of Ramanujan fellowship. Authors are also thankful to
603 University Grant Commission, New Delhi to provide JRF/SRF for this study.

604

605 **References**

606 Basu, S., Yadav, B. K., and Mathur, S. 2015. Enhanced bioremediation of BTEX contaminated
607 groundwater in pot-scale wetlands. *Environmental science and pollution Research*.
608 22(24), 20041-20049.

609 Brusseau, M. L., Zhang, Z., Nelson, N. T., Cain, R. B., Tick, G. R., and Oostrom, M. 2002.
610 Dissolution of non-uniformly distributed immiscible liquid: intermediate-scale
611 experiments and mathematical modeling. *Environmental science and technology*. 36(5),
612 1033-1041.

613 Cherry J.A; Parker B.L; Bradbury K.R; Eaton T.T; Gotkowitz M.G; Hart; Borchardt M.A.,
614 2004. Role of Aquitards in the Protection of Aquifers from Contamination: A “State of
615 the Science” Report, Published by the Awwa Research Foundation, Denver, CO 80235-
616 3098.

617 Chrysikopoulos, C.V., 1995. Three-dimensional analytical models of contaminant transport
618 from nonaqueous phase liquid pool dissolution in saturated subsurface formations. *Water*
619 *resource research*. 31, 1137–1145.

620 Chrysikopoulos, C.V., Voudrias, E.A., Fyrrillas, M.M., 1994. Modeling of contaminant
621 transport resulting from dissolution of nonaqueous phase liquid pools in saturated porous
622 media. *Transport in Porous Media* 16, 125–145.

623 Das, D. B. 2002. Hydrodynamic modelling for groundwater flow through permeable reactive
624 barriers. *Hydrological Processes*, 16(17), 3393-3418.

625 Das, D. B., and Mirzaei, M. 2012. Dynamic effects in capillary pressure relationships for two-
626 phase flow in porous media: Experiments and numerical analyses. *AIChE*
627 *Journal*, 58(12), 3891-3903.

628 Das, D. B., and Nassehi, V. 2003. Modeling of contaminants mobility in underground domains
629 with multiple free/porous interfaces. *Water Resources Research*, 39(3).

630 Dempster, H.S., Sherwood-Lollar, B., Feenstra, S., 1997. Tracing organic contaminants in
631 groundwater: a new methodology using compound-specific isotopic analysis.
632 *Environmental science and technology*. 31, 3193–3197.

633 Dobson, R., M.H. Schroth, and J. Zeyer. 2007. Effect of water-table fluctuation on dissolution
634 on and biodegradation of a multi-component, light nonaqueous-phase liquid. *Journal of*
635 *contaminant hydrology*. 94, 235–248.

636 Herzyk, A., Fillinger, L., Larentis, M., Qiu, S., Maloszewski, P., Hünninger, M., Schmidt, S.I.,
637 Stumpp, C., Marozava, S., Knappett, P.S. and Elsner, M., 2017. Response and recovery

638 of a pristine groundwater ecosystem impacted by toluene contamination—A meso-scale
639 indoor aquifer experiment. *Journal of contaminant hydrology*. 207, 17-30.

640 Illangasekare, T.H., E. J. Armbruster, D. N. Yates, 1995. Non-aqueous-phase fluids in
641 heterogeneous aquifers - Experimental study. *Journal of environmental engineering*. 121,
642 571-579.

643 Kamaruddin SA, Sulaiman WNA, Rahman NA, Zakaria MP, Mustaffar M, Sa'ari R., 2011. A
644 review of laboratory and numerical simulations of hydrocarbons migration in subsurface
645 environments. *Journal of environmental science and technology*. 4(3), 191–214.
646 doi:10.3923/jest.2011.191.214.

647 Kechavarzi C., Soga K., Illangasekare T. H., 2005. Two-dimensional laboratory simulation of
648 LNAPL infiltration and redistribution in the Vadose zone. *Journal contaminant*
649 *hydrology*. 76(3–4):211–233.

650 Kim, T. J., and C. V. Chrysikopoulos, 1999. Mass transfer correlations for nonaqueous phase
651 liquid pool dissolution in saturated porous media, *Water resource research*. 35(2), 449–
652 459.

653 Kumar, A., Datta, M., Nema, A. K., and Singh, R. K. 2016. An improved rating system for
654 assessing surface water contamination potential from MSW landfills. *Environmental*
655 *Modeling and Assessment*, 21(4), 489-505.

656 Lee, K. Y., and C. V. Chrysikopoulos, 1998. NAPL pool dissolution in stratified and
657 anisotropic porous formations, *J. Environmental engineering*. 124(9), 851–862.

658 Legout C, Molenat J, Hamon Y., 2009. Experimental and modeling investigation of unsaturated
659 solute transport with water-table fluctuation. *Vadose zone journal*. 8:21–31.

660 Lenhard R. J., Oostrom M, Dane J.H., 2004. A constitutive model for air- NAPL-water flow in
661 the vadose zone accounting for immobile, non-occluded (residual) NAPL in strongly
662 water-wet porous media. *Journal contaminant hydrology*. 71(1–4):261–282.

663 Mobile, M. A., Widdowson, M. A., and Gallagher, D. L. 2012. Multicomponent NAPL source
664 dissolution: Evaluation of mass-transfer coefficients. *Environmental science and*
665 *technology*. 46(18), 10047-10054.

666 Mustapha, H. I., Gupta, P. K., Yadav, B. K., van Bruggen, J. J. A., and Lens, P. N. L. 2018.
667 Performance evaluation of duplex constructed wetlands for the treatment of diesel
668 contaminated wastewater. *Chemosphere*, 205, 166-177.

669 Nambi, I.M., and Powers, S.E., 2000. NAPL dissolution in heterogeneous systems: an
670 experimental investigation in a simple heterogeneous system. *Journal contaminant*
671 *hydrology*. 44, 161–184.

672 Nambi, I.M., and Powers, S.E., 2003. Mass transfer correlations for nonaqueous phase liquid
673 dissolution from regions with high initial saturations. *Water resource research*. 39 (2).

674 Neale, C. N., Hughes, J. B., and Ward, C. H., 2000. Impacts of unsaturated zone properties on
675 oxygen transport and aquifer reaeration. *Groundwater*. 38(5), 784-794.

676 Nema, A. K., and Gupta, S. K. 1999. Optimization of regional hazardous waste management
677 systems: an improved formulation. *Waste Management*, 19(7-8), 441-451.

678 Nema, A. K., and Gupta, S. K. 2003. Multiobjective risk analysis and optimization of regional
679 hazardous waste management system. *Practice Periodical of Hazardous, Toxic, and*
680 *Radioactive Waste Management*, 7(2), 69-77.

681 Oostrom, M., Dane, J. H., and Wietsma, T. W., 2007. A review of multidimensional, multifluid,
682 intermediate-scale experiments: Flow behavior, saturation imaging, and tracer detection
683 and quantification. *Vadose zone journal*. 6(3), 610-637.

684 Oostrom, M., Hofstee, C., and Wietsma, T. W. 2006. LNAPLs do not always float: an example
685 case of a viscous LNAPL under variable water table conditions (No. PNNL-SA-48870).
686 Pacific Northwest National Laboratory (PNNL), Richland, WA (US), Environmental
687 Molecular Sciences Laboratory (EMSL).

688 Patterson B. M. and Davis G. B., 2009. Quantification of vapor intrusion pathways into a slab-
689 on-ground building under varying environmental conditions. *Environ Science and*
690 *Technology*. 43(3):650–656.

691 Picone, S., Grotenhuis, T., van Gaans, P., Valstar, J., Langenhoff, A., and Rijnaarts, H., 2013.
692 Toluene biodegradation rates in unsaturated soil systems versus liquid batches and their
693 relevance to field conditions. *Applied microbiology and biotechnology*. 97(17), 7887-
694 7898.

695 Power S.E. and Heermann S.E., 1999. Potential ground and surface water impacts, appendix
696 B: Modeling interface mass-transfer processes” presented in "A critical review: the effect
697 of ethanol in gasoline on the fate and transport of BTEX in the subsurface", Editors
698 Cannon G. and Rice D., UCRL-AR-135949 Vol.4, chapter 2.

699 Powers, S.E., Abriola, L.M., Dunkin, J.S., Weber, W.J., 1994a. Phenomenological model for
700 transient NAPL–water mass transfer processes. *Journal contaminant hydrology*. 16, 1–
701 33.

702 Powers, S.E., Abriola, L.M., Weber Jr., W.J., 1992a. An experimental investigation of
703 nonaqueous phase liquid dissolution in saturated subsurface systems: steady state mass
704 transfer rates. *Water resource research*. 28 (10), 2691 – 2705.

705 Powers, S.E., Abriola, L.M., Weber, W., 1994b. An experimental investigation of NAPL
706 dissolution in saturated subsurface systems: transient mass transfer rates. *Water resource*
707 *research*. 30, 321–332.

708 Powers, S.E., Abriola, L.M., Weber, W.J., 1992b. An experimental investigation of
709 nonaqueous phase liquid dissolution in saturated subsurface systems: steady state mass
710 transfer rates. *Water resource research*. 28 (10), 2691–2705.

711 Rivett, M.O., Wealthall, G.P., Dearden, R.A., McAlary, T.A., 2011. Review of unsaturated-
712 zone transport and attenuation of volatile organic compound (VOC) plumes leached from
713 shallow source zones. *Journal of contaminant hydrology* 123, 130-156.

714 Rolle, M., Eberhardt, C., Chiogna, G., Cirpka, O. A., and Grathwohl, P., 2009. Enhancement
715 of dilution and transverse reactive mixing in porous media: Experiments and model-
716 based interpretation. *Journal of contaminant hydrology*, 110(3-4), 130-142.

717 Saba, T.A., Illangasekare, T.H., 2000. Effect of ground-water flow dimensionality on mass
718 transfer from entrapped nonaqueous phase liquid contaminants. *Water resource research*.
719 36 (4), 971 – 979.

720 Sarikurt, D. A., Gokdemir, C., and Coptly, N. K., 2017. Sherwood correlation for dissolution of
721 pooled NAPL in porous media. *Journal of contaminant hydrology*. 206, 67-74.

722 Simunek, J., T. Vogel, and M.Th. van Genuchten., 1996. HYDRUS-2D code for simulating
723 water flow and solute transport in two-dimensional variably saturated media. Version
724 1.0. USDA/ARS, U.S. Salinity Lab., Riverside, CA.

725 Šimunek, J., Van Genuchten, M. T., and Šejna, M. (2012). HYDRUS: Model use, calibration,
726 and validation. *Transactions of the ASABE*, 55(4), 1263-1274.

727 Sulaymon, A., and H.A. Gzar., 2011. Experimental investigation and numerical modelling of
728 light non-aqueous phase liquid dissolution and transport in a saturated zone of the soil.
729 *Journal of Hazardous Materials*. (186), 1601–1614.

- 730 Vasudevan, M., G. Suresh Kumar, N. Indumathi M., 2014. Numerical study on
731 kinetic/equilibrium behaviour of dissolution of toluene under variable subsurface
732 conditions. *European journal of environmental and civil Engineering*. 18(9), pp.1070–
733 1093.
- 734 Yadav B.K., and Hassanizadeh S.M., 2011. An overview of biodegradation of LNAPLs in
735 coastal (semi)-arid environment. *Water air soil pollution*. 220, 225-239.
- 736 Yadav B.K., Ansari FA, Basu S, Mathur A., 2013. Remediation of LNAPL contaminated
737 groundwater using plant-assisted biostimulation and bioaugmentation Methods”. *Water*
738 *air soil pollution*. 225, 1793.
- 739 Yadav, B.K., Shrestha, S.R. and Hassanizadeh, S.M., 2012. Biodegradation of toluene under
740 seasonal and diurnal fluctuations of soil-water temperature. *Water, air, and soil pollution*,
741 223(7), pp.3579–3588.
- 742 Zhang Q, Wang G.C., Sugiura N, Utsumi M, Zhang ZY, Yang YN., 2014. Distribution of
743 petroleum hydrocarbons in soils and the underlying unsaturated subsurface at an
744 abandoned petrochemical site, North China. *Hydrological process*. 28, 2185–2191.
- 745 Zhou, A. X., Zhang, Y. L., Dong, T. Z., Lin, X. Y., and Su, X. S., 2015. Response of the
746 microbial community to seasonal groundwater level fluctuations in petroleum
747 hydrocarbon-contaminated groundwater. *Environmental science and pollution*
748 *research*. 22(13), 10094-10106.

Assessment of LNAPL in subsurface under fluctuating groundwater table using 2D sand tank experiments

Gupta, Pankaj Kumar

2019-06-24

Attribution-NonCommercial 4.0 International

Gupta PK, Yadav B, Yadav BK. Assessment of LNAPL in subsurface under fluctuating groundwater table using 2D sand tank experiments. *Journal of Environmental Engineering*, Volume 145, Issue 9, September 2019

[https://doi.org/10.1061/\(ASCE\)EE.1943-7870.0001560](https://doi.org/10.1061/(ASCE)EE.1943-7870.0001560)

Downloaded from CERES Research Repository, Cranfield University